Table 1. Lymphoma incidence in HCV-expressing and control mice

HCV expression	Mouse genotype	No.	Incident B lymphoma, number (%)	Incident T lymphoma, number (%)
+	RzCD19Cre	72	18 (25.0)	3 (4.1)
−	Rz	34	1 (2.9)	1 (2.9)
−	CD19Cre	22	2 (9.1)	1 (4.5)
−	WT	12	1 (8.3)	1 (8.3)

(mouse ID Nos. 5, 6, 7) of MxCre/CN2-29 mice but not in spleens of the CN2-29 mouse (mouse ID No. 1, Figure 3B). After 12 months, the MxCre/CN2-29 mice developed B-cell lymphomas in the spleen at a high incidence (33.3%: 3/9), whereas the CN2-29 mice did not (0/13; supplemental Figure 3C), indicating that the development of B-cell lymphomas in HCV transgenic mice occurred similarly to RzCD19Cre mice. MxCre/CN2-29 mice also developed hepatocellular carcinomas (10%, 360 days, 17%, 480 days, 50%, 600 days after onset of HCV expression; Sekiguchi et al, submitted).

The results obtained in 2 HCV transgenic mouse strains indicate that the expression of the HCV gene or the proteins indeed induces the spontaneous development of B-cell lymphomas irrespective of the integrated site in the mouse genome.

The levels of cytokines and chemokines in B-cell lymphomas and other tumors and in tumor-free control mice

Abnormal induction of cytokine production occurs in HCV-associated non-Hodgkin lymphomas[27,28] and in patients with

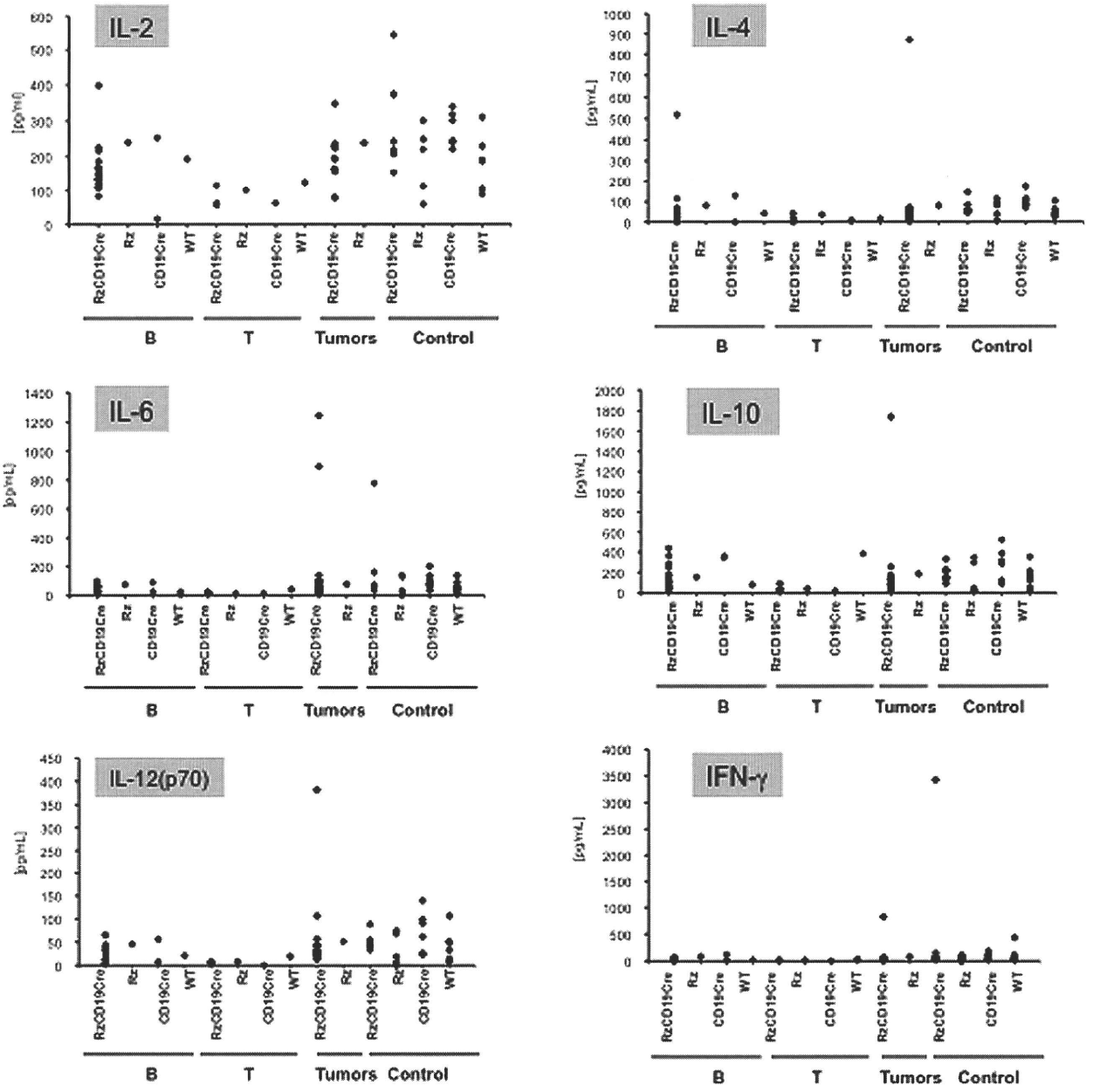

Figure 3. Analysis of serum cytokine levels using a multisuspension array system. The serum concentration levels of IL-2, IL-4, IL-6, IL-10, IL-12(p70), and IFN-γ were measured in RzCD19Cre mice with B-cell lymphomas (B), T-cell lymphomas (T), and other tumors (mammary tumor, sarcoma, and hepatocellular carcinoma) and in tumor-free RzCD19Cre, Rz, CD19Cr,e and WT mice.

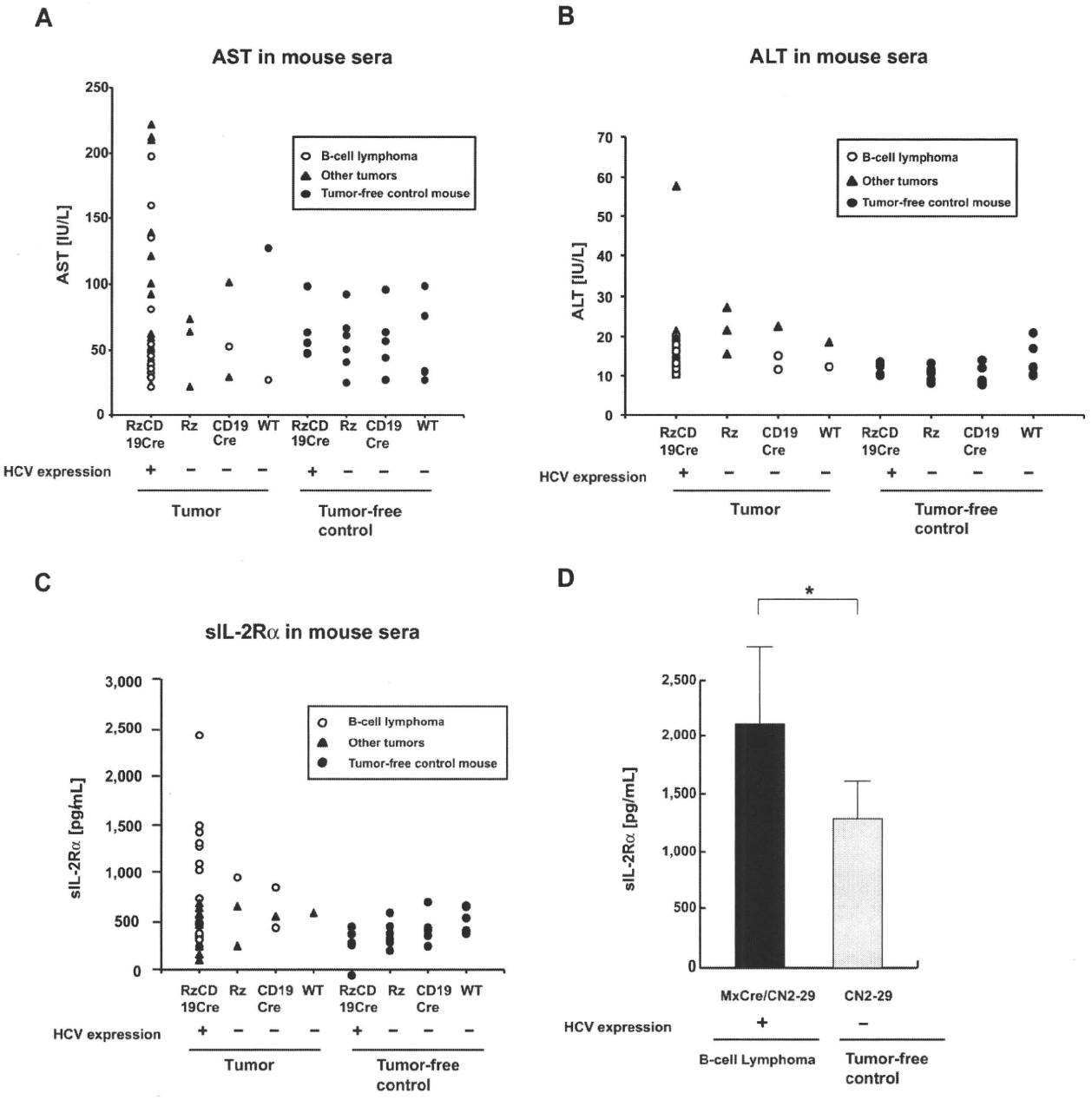

Figure 4. Serum titers of AST, ALT and soluble IL-2Rα in transgenic and control mice lacking or harboring B-cell lymphomas. (A-B) The AST (A) and ALT (B) assays were performed on serum samples from tumor-free control mice and the RzCD19Cre, Rz, CD19Cre and WT mice with or without B-cell lymphomas or other tumors. (C) ELISA analysis was performed to determine the sIL-2Rα concentration in serum samples from tumor-free control mice and the RzCD19Cre, Rz, CD19Cre, and WT mice with or without B-cell lymphomas or other tumors. (D) Concentration of soluble IL-2Rα in sera from transgenic (MxCre/CN2-29 or CN2-29) mice with or without B-cell lymphomas (*$P < .05$).

chronic hepatitis.[29,30] Therefore, we examined tumor cytokine and chemokine levels using a multisuspension array system. The levels of IL-2, IL-4, IL-6, IL-10, IL-12(p70), and IFN-γ (Figure 3), which may have a link with lymphoproliferation[14] or lymphoma[28,31] induced by HCV, and IL-1α, IL-1β, IL-3, IL-5, IL-9, IL-12(p40), IL-13, IL-17, Eotaxin, granulocyte-CSF, granulocyte–macrophage–CSF, KC, monocyte chemotactic protein-1, MIP-1α, MIP-1β, Regulated upon Activation, Normal T-cell Expressed, and Secreted, tumor necrosis factor-α, IL-15, fibroblast growth factor-basic, leukemia inhibitory factor, macrophage-CSF, human monokine induced by gamma interferon, MIP-2, platelet-derived growth factorβ and vascular endothelial growth factor (supplemental Figure 4) were measured in sera from mice with B-cell lymphomas, T-cell lymphomas, and other tumors and in sera from tumor-free RzCD19Cre, Rz, CD19Cre, and WT control mice. The levels of these cytokines and chemokines in sera from tumor-bearing RzCD19Cre mice with B-cell lymphomas were not significantly different from those of the control groups, and thus, changes in the expression of these cytokines and chemokines were not strictly correlated with the occurrence of B-cell lymphoma in RzCD19Cre mice.

The levels of amino transferases and sIL-2Rα in mice lacking or harboring B-cell lymphomas

We also examined the levels of AST and ALT in the RzCD19Cre, Rz, CD19Cre, and WT mice. There were no significant differences in the levels of AST and ALT in the sera of mice lacking or harboring B-cell lymphomas ($P > .05$; Figure 4A-B; AST:

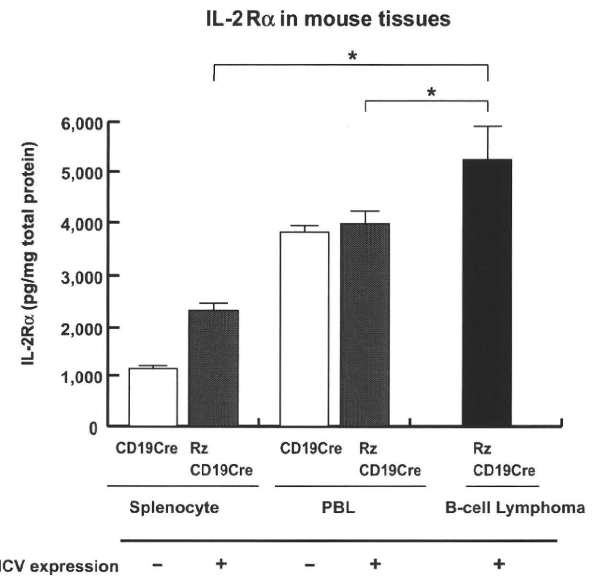

Figure 5. Levels of IL-2Rα in transgenic and control mice lacking or harboring B-cell lymphomas. The expression level of IL-2Rα in splenocytes and PBLs from CD19Cre and RzCD19Cre mice and in B-cell lymphomas from RzCD19Cre mice was measured by ELISA. IL-2Rα levels per total protein are indicated (picograms per milligram). Data from quadruplicate samples are shown as the mean ± SD (*$P < .05$).

RzCD19Cre mice with B-cell lymphomas, 72.2 ± 60.5 IU/L; normal controls, 55.2 ± 23.0 IU/L and ALT: RzCD19Cre mice with B-cell lymphomas, 14.2 ± 3.1 IU/L; normal controls, 11.5 ± 3.0 IU/L).

Finally, we examined the level of sIL-2Rα in the sera of the RzCD19Cre mice with B-cell lymphomas; sIL-2Rα is generated by proteolytic cleavage of IL-2Rα (CD25) residing on the surface of activated T and natural killer cells, monocytes, and certain tumor cells.[24,32] The average sIL-2Rα level in the RzCD19Cre mice with B-cell lymphomas (830.3 ± 533.0 pg/mL) was significantly higher than that in the tumor-free control groups, including the RzCD19Cre, Rz, CD19Cre and WT mice (499.9 ± 110.2 pg/mL; $P < .0057$; Figure 4C). The average sIL-2Rα levels in other tumor-containing groups (430.46 ± 141.15 pg/mL) were not significantly different from those in the tumor-free control groups ($P > .05$; Figure 4C). Moreover, all RzCD19Cre mice with a relatively high level of sIL-2Rα (> 1000 pg/mL) presented with B-cell lymphomas (Figure 4C).

We also examined the level of sIL-2Rα in MxCre/CN2-29 mice and observed a significant increase in sIL-2Rα in mice that expressed HCV and that had B-cell lymphomas compared with tumor-free control (CN2-29) mice (Figure 4D).

Expression of IL-2Rα in B-cell lymphomas of the RzCD19Cre mice

To examine whether sIL-2Rα was derived from lymphoma tissues, we quantified IL-2Rα concentrations in splenocytes, PBLs and B-cell lymphoma tissues (Figure 5). The concentration of IL-2Rα was significantly higher in splenocytes from RzCD19Cre mice compared with those from CD19Cre mice; the concentration was even higher in B-cell lymphoma tissues than in splenocytes from RzCD19Cre mice (Figure 5). These results strongly suggest that B-cell lymphomas directly contribute to the elevated serum concentrations of sIL-2Rα in RzCD19Cre mice.

Discussion

We have established HCV transgenic mice that have a high incidence of spontaneous B-cell lymphomas. In this animal model, the HCV transgene is expressed during the embryonic stage, and these RzCD19Cre mice are expected to be immunotolerant to the HCV transgene product. Thus, the results from this study reveal the potential for the HCV gene to induce B-cell lymphomas without inducing host immune responses against the HCV gene product. A retrospective study indicated that viral elimination reduced the incidence of malignant lymphoma in patients infected with HCV.[33] The results in our study may be consistent with this retrospective observation, indicating the significance of the direct effect of HCV infection on B-cell lymphoma development. Another HCV transgenic mouse strain (MxCre/CN2-29) showed the similarly high incidence of B-cell lymphoma, which strongly supported that development of B-cell lymphomas occurred by the expression of HCV transgene.

Recent findings have revealed the significance of B lymphocytes in HCV infection of liver-derived hepatoma cells.[34] In 4.2% of the RzCD19Cre mice, CD45R-positive intrahepatic lymphomas were identified, and infiltration of B cells into the hepatocytes was frequently observed (data not shown). These phenomena suggest that HCV could modify the in vivo tropism of B cells. The RzCD19Cre mouse is a powerful model system to address these mechanisms in vivo.

As a circulating membrane receptor, sIL-2Rα is localized in lymphoid cells and some other types of cancer cells and is highly expressed in several cancers[35-40] and autoimmune diseases.[41] Recent findings indicate a link between sIL-2Rα levels and hepatocellular carcinoma in Egyptian patients.[42] Appearing on the surface of leukemic cells derived from B and pre-B lymphocytes and other leukemic cells, IL-2Rα is one of the subunits of the IL-2 receptor, which is composed of an α chain (CD25), a β chain (CD122), and a γ chain (CD132).[43] IL-2R ectodomains are thought to be proteolytically cleaved from the cell surface[34,44,45] instead of produced as a result of posttranscriptional splicing.[24] In RzCD19Cre splenocytes, the level of IL-2Rα was higher than that in splenocytes from CD19Cre mice; however, serum concentrations of sIL-2Rα in RzCD19Cre mice without B-cell lymphomas did not show significant differences compared with other control groups (Rz, CD19Cre, and WT). These results indicate the possibility that HCV may increase IL-2Rα expression on B-cells; proteolytic cleavage of IL-2Rα was increased after B-cell lymphoma development in the RzCD19Cre mouse. The detailed mechanism that induces IL-2Rα as a result of HCV expression is still unclear at present, but we have found previously that the HCV core protein induces IL-10 expression in mouse splenocytes.[14] IL-10 up-regulates the expression of IL-2Rα (Tac/CD25) on normal and leukemic B lymphocytes,[46] and therefore, through IL-10, the HCV core protein might induce IL-2Rα in B cells of the RzCD19Cre mouse.

In conclusion, this study established an animal model that will likely provide critical information for the elucidation of molecular mechanism(s) underlying the spontaneous development of B-cell non-Hodgkin lymphoma after HCV infection. This knowledge should lead to therapeutic strategies to prevent the onset and/or progression of B-cell lymphomas.

Acknowledgments

We thank Dr T. Ito for assistance with pathology characterization and Dr T. Munakata for valuable comments.

This work was supported by grants from the Ministry of Health and Welfare of Japan and the Cooperative Research Project on Clinical and Epidemiologic Studies of Emerging and Re-emerging Infectious Diseases.

Authorship

Contribution: K.T.-K. conceived of the project; K.K., M.K., and K.T.-K. designed the studies; Y.K., S.S., M. Saito, K.T., M. Satoh, M.T., and K.T.-K. performed experiments and analyses; N.S. and Y.H. provided scientific advice; and K.T.-K. wrote the manuscript.

Conflict-of-interest disclosure: The authors declare no competing financial interests.

Correspondence: Kyoko Tsukiyama-Kohara, Department of Experimental Phylaxiology, Faculty of Life Sciences, Kumamoto University, Kumamoto 860-8556, Japan; e-mail: kkohara@kumamoto-u.ac.jp.

References

1. Ferri C, Monti M, La Civita L, et al. Infection of peripheral blood mononuclear cells by hepatitis C virus in mixed cryoglobulinemia. *Blood.* 1993; 82(12):3701-3704.
2. Saito I, Miyamura T, Ohbayashi A, et al. Hepatitis C virus infection is associated with the development of hepatocellular carcinoma. *Proc Natl Acad Sci U S A.* 1990;87(17):6547-6549.
3. Simonetti RG, Camma C, Fiorello F, et al. Hepatitis C virus infection as a risk factor for hepatocellular carcinoma in patients with cirrhosis. A case-control study. *Ann Intern Med.* 1992;116(2):97-102.
4. Silvestri F, Pipan C, Barillari G, et al. Prevalence of hepatitis C virus infection in patients with lymphoproliferative disorders. *Blood.* 1996;87(10): 4296-4301.
5. Ascoli V, Lo Coco F, Artini M, Levrero M, Martelli M, Negro F. Extranodal lymphomas associated with hepatitis C virus infection. *Am J Clin Pathol.* 1998;109(5):600-609.
6. Mele A, Pulsoni A, Bianco E, et al. Hepatitis C virus and B-cell non-Hodgkin lymphomas: an Italian multicenter case-control study. *Blood.* 2003; 102(3):996-999.
7. Dammacco F, Sansonno D, Piccoli C, Racanelli V, D'Amore FP, Lauletta G. The lymphoid system in hepatitis C virus infection: autoimmunity, mixed cryoglobulinemia, and overt B-cell malignancy. *Semin Liver Dis.* 2000;20(2):143-157.
8. Gisbert JP, Garcia-Buey L, Pajares JM, Moreno-Otero R. Prevalence of hepatitis C virus infection in B-cell non-Hodgkin's lymphoma: systematic review and meta-analysis. *Gastroenterology.* 2003;125(6):1723-1732.
9. Negri E, Little D, Boiocchi M, La Vecchia C, Franceschi S. B-cell non-Hodgkin's lymphoma and hepatitis C virus infection: a systematic review. *Int J Cancer.* 2004;111(1):1-8.
10. Pileri P, Uematsu Y, Campagnoli S, et al. Binding of hepatitis C virus to CD81. *Science.* 1998; 282(5390):938-941.
11. Rosa D, Saletti G, De Gregorio E, et al. Activation of naive B lymphocytes via CD81, a pathogenetic mechanism for hepatitis C virus-associated B lymphocyte disorders. *Proc Natl Acad Sci U S A.* 2005;102(51):18544-18549.
12. Wakita T, Taya C, Katsume A, et al. Efficient conditional transgene expression in hepatitis C virus cDNA transgenic mice mediated by the Cre/loxP system. *J Biol Chem.* 1998;273(15):9001-9006.
13. Machida K, Tsukiyama-Kohara K, Seike E, et al. Inhibition of cytochrome c release in Fas-mediated signaling pathway in transgenic mice induced to express hepatitis C viral proteins. *J Biol Chem.* 2001;276(15):12140-12146.
14. Machida K, Tsukiyama-Kohara K, Sekiguch S, et al. Hepatitis C virus and disrupted interferon signaling promote lymphoproliferation via type II CD95 and interleukins. *Gastroenterology.* 2009; 137(1):285-296,296 e281-211.
15. Lerat H, Rumin S, Habersetzer F, et al. In vivo tropism of hepatitis C virus genomic sequences in hematopoietic cells: influence of viral load, viral genotype, and cell phenotype. *Blood.* 1998; 91(10):3841-3849.
16. Karavattathayyil SJ, Kalkeri G, Liu HJ, et al. Detection of hepatitis C virus RNA sequences in B-cell non-Hodgkin lymphoma. *Am J Clin Pathol.* 2000;113(3):391-398.
17. Rickert RC, Roes J, Rajewsky K. B lymphocyte-specific, Cre-mediated mutagenesis in mice. *Nucleic Acids Res.* 1997;25(6):1317-1318.
18. Tanaka T, Lau JY, Mizokami M, et al. Simple fluorescent enzyme immunoassay for detection and quantification of hepatitis C viremia. *J Hepatol.* 1995;23(6):742-745.
19. Tsukiyama-Kohara K, Tone S, Maruyama I, et al. Activation of the CKI-CDK-Rb-E2F pathway in full genome hepatitis C virus-expressing cells. *J Biol Chem.* 2004;279(15):14531-14541.
20. Nishimura T, Kohara M, Izumi K, et al. Hepatitis C virus impairs p53 via persistent overexpression of 3beta-hydroxysterol Delta24-reductase. *J Biol Chem.* 2009;284(52):36442-36452.
21. Tsukiyama-Kohara K, Poulin F, Kohara M, et al. Adipose tissue reduction in mice lacking the translational inhibitor 4E-BP1. *Nat Med.* 2001; 7(10):1128-1132.
22. Fujimura S, Xing Y, Takeya M, et al. Increased expression of germinal center-associated nuclear protein RNA-primase is associated with lymphomagenesis. *Cancer Res.* 2005;65(13):5925-5934.
23. Miyazaki T, Kato I, Takeshita S, Karasuyama H, Kudo A. Lambda5 is required for rearrangement of the Ig kappa light chain gene in pro-B cell lines. *Int Immunol.* 1999;11(8):1195-1202.
24. Rubin LA, Galli F, Greene WC, Nelson DL, Jay G. The molecular basis for the generation of the human soluble interleukin 2 receptor. *Cytokine.* 1990;2(5):330-336.
25. Tsukiyama-Kohara K, Iizuka N, Kohara M, Nomoto A. Internal ribosome entry site within hepatitis C virus RNA. *J Virol.* 1992;66(3):1476-1483.
26. Jaffe ES, Harris NL, Stein H, Isaacson PG. Classification of lymphoid neoplasms: the microscope as a tool for disease discovery. *Blood.* 2008; 112(12):4384-4399.
27. el-Din HM, Attia MA, Hamza MR, Khaled HM, Thoraya MA, Eisa SA. Hepatitis C Virus and related changes in immunologic parameters in non Hodgkin's lymphoma patients. *Egypt J Immunol.* 2004;11(1):55-64.
28. Feldmann G, Nischalke HD, Nattermann J, et al. Induction of interleukin-6 by hepatitis C virus core protein in hepatitis C-associated mixed cryoglobulinemia and B-cell non-Hodgkin's lymphoma. *Clin Cancer Res.* 2006;12(15):4491-4498.
29. Mizuochi T, Ito M, Takai K, Yamaguchi K. Differential susceptibility of peripheral blood CD5+ and CD5− B cells to apoptosis in chronic hepatitis C patients. *Biochem Biophys Res Commun.* 2009; 389(3):512-515.
30. Bansal AS, Bruce J, Hogan PG, Prichard P, Powell EE. Serum soluble CD23 but not IL8, IL10, GM-CSF, or IFN-gamma is elevated in patients with hepatitis C infection. *Clin Immunol Immunopathol.* 1997;84(2):139-144.
31. Barrett L, Gallant M, Howley C, et al. Enhanced IL-10 production in response to hepatitis C virus proteins by peripheral blood mononuclear cells from human immunodeficiency virus-monoinfected individuals. *BMC Immunol.* 2008;9:28.
32. Rubin LA, Kurman CC, Fritz ME, et al. Soluble interleukin 2 receptors are released from activated human lymphoid cells in vitro. *J Immunol.* 1985;135(5):3172-3177.
33. Kawamura Y, Ikeda K, Arase Y, et al. Viral elimination reduces incidence of malignant lymphoma in patients with hepatitis C. *Am J Med.* 2007; 120(12):1034-1041.
34. Stamataki Z, Shannon-Lowe C, Shaw J, et al. Hepatitis C virus association with peripheral blood B lymphocytes potentiates viral infection of liver-derived hepatoma cells. *Blood.* 2009;113(3): 585-593.
35. Wasik MA, Sioutos N, Tuttle M, Butmarc JR, Kaplan WD, Kadin ME. Constitutive secretion of soluble interleukin-2 receptor by human T cell lymphoma xenografted into SCID mice. Correlation of tumor volume with concentration of tumor-derived soluble interleukin-2 receptor in body fluids of the host mice. *Am J Pathol.* 1994;144(5): 1089-1097.
36. Tsai MH, Chiou SH, Chow KC. Effect of platelet activating factor and butyrate on the expression of interleukin-2 receptor alpha in nasopharyngeal carcinoma cells. *Int J Oncol.* 2001;19(5):1049-1055.
37. Yano T, Yoshino I, Yokoyama H, et al. The clinical significance of serum soluble interleukin-2 receptors in lung cancer. *Lung Cancer.* 1996;15(1):79-84.
38. Tesarova P, Kvasnicka J, Umlaufova A, Homolkova H, Jirsa M, Tesar V. Soluble TNF and IL-2 receptors in patients with breast cancer. *Med Sci Monit.* 2000;6(4):661-667.
39. Maccio A, Lai P, Santona MC, Pagliara L, Melis GB, Mantovani G. High serum levels of soluble IL-2 receptor, cytokines, and C reactive protein correlate with impairment of T cell response in patients with advanced epithelial ovarian cancer. *Gynecol Oncol.* 1998;69(3):248-252.
40. Matsumoto T, Furukawa A, Sumiyoshi Y, Akiyama KY, Kanayama HO, Kagawa S. Serum levels of soluble interleukin-2 receptor in renal cell carcinoma. *Urology.* 1998;51(1):145-149.
41. Pountain G, Hazleman B, Cawston TE. Circulating levels of IL-1beta, IL-6 and soluble IL-2 receptor in polymyalgia rheumatica and giant cell arteritis and rheumatoid arthritis. *Br J Rheumatol.* 1998;37(7):797-798.
42. Zekri AR, Alam El-Din HM, Bahnassy AA, et al. Serum levels of soluble Fas, soluble tumor necrosis factor-receptor II, interleukin-2 receptor and interleukin-8 as early predictors of hepatocellular carcinoma in Egyptian patients with hepatitis C virus genotype-4. *Comp Hepatol.* 2010:9(1):1.
43. Sheibani K, Winberg CD, van de Velde S, Blayney DW, Rappaport H. Distribution of lymphocytes with interleukin-2 receptors (TAC antigens) in reactive lymphoproliferative processes, Hodgkin's disease, and non-Hodgkin's lymphomas. An immunohistologic study of 300 cases. *Am J Pathol.* 1987;127(1):27-37.
44. Robb RJ, Rusk CM. High and low affinity receptors for interleukin 2: implications of pronase, phorbol ester, and cell membrane studies upon the basis for differential ligand affinities. *J Immunol.* 1986;137(1):142-149.
45. Sheu BC, Hsu SM, Ho HN, Lien HC, Huang SC, Lin RH. A novel role of metalloproteinase in cancer-mediated immunosuppression. *Cancer Res.* 2001;61(1):237-242.
46. Fluckiger AC, Garrone P, Durand I, Galizzi JP, Banchereau J. Interleukin 10 (IL-10) up-regulates functional high affinity IL-2 receptors on normal and leukemic B lymphocytes. *J Exp Med.* 1993; 178(5):1473-1481.

JOURNAL OF CLINICAL MICROBIOLOGY, Nov. 2010, p. 3843–3851 Vol. 48, No. 11
0095-1137/10/$12.00 doi:10.1128/JCM.00415-10

Detection of Hepatitis B and C Viruses in Almost All Hepatocytes by Modified PCR-Based *In Situ* Hybridization▽

Hideko Nuriya,[1] Kazuaki Inoue,[1,2] Takeshi Tanaka,[3] Yukiko Hayashi,[4] Tsunekazu Hishima,[4] Nobuaki Funata,[4] Kyosuke Kaji,[5] Seishu Hayashi,[3] Shuichi Kaneko,[5] and Michinori Kohara[1]*

Department of Microbiology and Cell Biology, Tokyo Metropolitan Institute of Medical Science, 2-1-6 Kamikitazawa, Setagaya-ku, Tokyo 156-0057, Japan[1]; Division of Gastroenterology, Showa University Fujigaoka Hospital, 1-30 Aoba-ku, Fujigaoka, Yokohama 227-8501, Japan[2]; Liver Unit, Tokyo Metropolitan Komagome Hospital, 3-18-22 Honkomagome, Bunkyo-ku, Tokyo 113-8613, Japan[3]; Department of Pathology, Tokyo Metropolitan Komagome Hospital, 3-18-22 Honkomagome, Bunkyo-ku, Tokyo 113-8613, Japan[4]; and Department of Gastroenterology, Kanazawa University Graduate School of Medical Science, Ishikawa 920-8641, Japan[5]

Received 28 February 2010/Returned for modification 22 April 2010/Accepted 16 August 2010

Although PCR-based *in situ* hybridization (PCR-ISH) can be used to determine the distribution and localization of pathogens in tissues, this approach is hampered by its low specificity. Therefore, we used a highly specific and sensitive PCR-ISH method to reveal the lobular distribution and intracellular localization of hepatitis B virus (HBV) and HCV in chronic liver disease and to clarify the state of persistent HBV and HCV infection in the liver. HBV genomic DNA was detected in almost all hepatocytes, whereas HBV RNA or protein was differentially distributed only in a subset of the HBV DNA-positive region. Further, HCV genomic RNA was detected in almost all hepatocytes and was localized to the cytoplasm. HCV RNA was also detected in the epithelium of the large bile duct but not in endothelial cells, portal tracts, or sinusoidal lymphocytes. In patients with HBV and HCV coinfection, HCV RNA was localized to the noncancerous tissue, whereas HBV DNA was found only in the cancerous tissue. Using this novel PCR-ISH method, we could visualize the staining pattern of HBV and HCV in liver sections, and we obtained results consistent with those of real-time detection (RTD)-PCR analysis. In conclusion, almost all hepatocytes are infected with HBV or HCV in chronic liver disease; this finding implies that the viruses spreads throughout the liver in the chronic stage.

Hepatitis B virus (HBV) and hepatitis C virus (HCV) are the primary causative agents of chronic liver disease (2, 9, 17). HBV infection remains a global health problem; it is estimated that 350 million individuals are persistently infected with the virus and that approximately 15% to 25% of these individuals will die due to the sequelae of the infection (23, 29). Further, more than 170 million people are infected with HCV worldwide (21). HCV has a single-stranded RNA genome (8, 19), does not have canonical oncogenes, and can easily establish chronic infection without integration into the host genome (3, 20), resulting in hepatic steatosis and hepatocellular carcinoma (HCC) (28). The viruses share a similar route of transmission, such as via the transfusion of infected blood or body fluids or use of contaminated needles.

Several studies have shown that 10% to 35% of the individuals infected with HBV also have HCV infection, although the prevalence varies depending on the population studied (4, 32, 34). The relationship between coinfection and acceleration of malignant transformation remains unclear, but HBV and HCV coinfection seems to alter the natural history of both HBV-related and HCV-related liver disease (2, 12). HCV has been shown to inhibit HBV gene expression (7, 15). The high prevalence of occult HBV infection may indicate that HCV also inhibits HBV replication (34). Most epidemiological studies of HBV have been performed by using diagnostic serological assays (16). We recently used a novel, highly sensitive diagnostic PCR method to demonstrate that the HBV genome is detectable in the sera of a substantial proportion of patients with chronic HCV infection who are seronegative for the standard HBV-related markers (1, 34). Further, we reported the levels of HBV DNA and HCV RNA in cancerous and noncancerous liver tissue using real-time detection (RTD)-PCR (34). RTD-PCR is an accurate assay method, but it can determine the levels of genomic DNA and RNA only in homogenized tissue. In this study, we developed a PCR-based *in situ* hybridization (PCR-ISH) method for detecting and visualizing HBV DNA, HBV RNA, and HCV RNA and comparing their protein expression patterns, with the aim to reveal the lobular distribution and intracellular localization of HBV and HCV in chronic liver disease and to clarify the state of persistent HBV and HCV infection in the liver.

MATERIALS AND METHODS

Patients. Twenty-nine patients were admitted to Tokyo Metropolitan Komagome Hospital for the treatment of hepatic tumors. Of these patients, 14 were considered to have chronic HCV infection (persistently positive results for HCV antibody), 8 were diagnosed with chronic hepatitis B (persistently positive results for HBV surface antigen [HBsAg]), and 7 showed negative results for both viral markers but had metastatic liver cancer (6 with colonic cancer and 1 with gastric cancer). We used four samples from seven patients as controls for PCR-ISH and four samples from seven patients as controls for reverse transcriptase PCR (RT-PCR)–ISH (Table 1). Of the 14 patients with chronic hepatitis C, two showed positive results for HBV DNA by RTD-PCR. HBsAg and second-generation HCV antibody were measured by using enzyme-linked immunosor-

* Corresponding author. Mailing address: Department of Microbiology and Cell Biology, The Tokyo Metropolitan Institute of Medical Science, 2-1-6, Kamikitazawa, Setagaya-ku, Tokyo 156-8506, Japan. Phone: 81-3-5316-3232. Fax: 81-3-5316-3137. E-mail: kohara-mc@igakuken.or.jp.

▽ Published ahead of print on 25 August 2010.

TABLE 1. Patient profiles and results of the present study

Patient no.	Age (yr)	Gender[a]	HCV antibody	HBs Ag	Liver histology	RT-PCR–ISH HCV	PCR-ISH HBV	Serum HBV DNA (copies/ml)[b]	Serum HCV RNA		IFN treatment	Note
									Copies/ml	KIU/ml[d]		
1	53	M	−	+	A2F3		+	1.1×10^2			−	
2	42	M	−	+	A2F2		+	4.0×10^5			−	Fig. 2A
3	43	M	−	+	A2F3		+	1.6×10^7			−	
4	53	M	−	+	A2F4		+	6.4×10^3			−	Fig. 1A
5	55	M	−	+	A2F3		+	1.0×10^3			−	Fig. 3A
6	54	M	−	+	A2F4	−	+	NT[c]			−	
7	31	M	−	+	A3F3		+	3.0×10^9			+	
8	61	F	−	+	A3F3		+	NT			−	
9	63	M	+	−	A3F4	+	−		5.6×10^6		−	Fig. 4D
10	56	M	+	−	A2F3	+	−		NT		+	
11	67	F	+	−	A3F4	−	−		NT		−	
12	73	M	+	−	A2F4	+			1.2×10^6		−	Fig. 1B
13	68	F	+	−	A3F4	+			1.1×10^6		−	
14	76	F	+	−	A2F4	+			9.5×10^5		−	Fig. 4A
15	62	M	+	−	A2F3	+			7.2×10^5		−	
16	65	M	+	−	A3F4	+			NT		−	
17	60	F	+	−	A3F4	+				41	−	
18	48	F	+	−	A2F1	+			7.6×10^6	>850	−	Fig. 4C
19	43	M	+	−	A2F3	+				389	−	
20	59	M	+	−	A2F3	+				>850	−	
21	72	F	+	−	A2F4	+	+	3.9×10^1	5.0×10^7			Fig. 5
22	69	M	+	−	A2F3	+	+	5.0×10^1	3.0×10^7			
23	69	M	−	−	Normal	−	−					Gastric cancer
24	58	M	−	−	Normal		−					Colon cancer
25	58	M	−	−	Normal	−						Colon cancer
26	59	F	−	−	Normal	−						Colon cancer
27	65	M	−	−	Normal	−						Colon cancer
28	47	M	−	−	Normal		−					Colon cancer
29	81	F	−	−	Normal		−					Colon cancer

[a] M, male; F, female.
[b] Serum HBV DNA was positive in patients 21 and 22.
[c] NT, not tested.
[d] KIU, kilo international units.

bent assay (ELISA) kits (Abbott Laboratories, Chicago, IL, and International Reagent Corp., Kobe, Japan, respectively). All 29 patients underwent hepatic resection. Histological evaluation of the liver was carried out according to the METAVIR scoring system (3).

Ethical approval. The Institutional Review Board of Tokyo Metropolitan Komagome Hospital approved the study. Written informed consent was obtained from all the subjects.

Sample preparation. The liver tissue samples for HBV DNA detection were fixed in 10% buffered formalin (pH 7.4) for 18 h, embedded in paraffin, cut into 6-μm-thick sections, and mounted on silane-coated glass slides for use with a GeneAmp *in situ* PCR system 1000 unit (Applied Biosystems, Foster City, CA). The slides were washed thrice in xylene for 8 min at each washing, rinsed thrice in 99.5% ethanol and 75% ethanol for 5 min at each rinsing, and rehydrated in distilled water for deparaffinization. For detecting HBV mRNA and HCV RNA, OCT-embedded frozen liver tissue samples were cut into 10-μm-thick sections and mounted on silane-coated glass slides. They were then fixed in 10% buffered formalin (pH 7.4) for 17 to 21 h, rinsed twice in distilled water treated with 0.01% diethylpyrocarbonate (DEPC) for 2 min at each rinse, rinsed in 99.5% ethanol for 1 min, and then air dried and stored at −80°C until use. The tissue sections on the glass slides were digested with proteinase K (1 to 30 μg/ml and 1 to 200 μg/ml for the noncancerous and cancerous regions of the paraffin-embedded sections, respectively; 0.008 to 1.0 μg/ml for the frozen sections) in 50 mM Tris (pH 7.5) at 37°C for 30 min in a humidified chamber. Subsequently, proteinase K was inactivated at 97°C for 10 min, and then the sections were rinsed with distilled water, dehydrated in 99.5% ethanol, and air dried.

Primers and probes for PCR-ISH and RT-PCR–ISH. The primers used to amplify the S and X regions of HBV and the 5′ untranslated region (5′-UTR) of HCV as well as the corresponding probes are listed in Table 2. We created a digoxigenin (DIG)-dUTP tail at the 3′ end of the 5′-DIG probe using a DNA tailing kit (Roche, Basel, Switzerland).

PCR-ISH for detecting HBV DNA. PCR was performed by using one of two sets of antisense and sense primers complementary to the sequences located in the S and X regions of HBV. The PCR mixture contained 10 mM Tris-HCl (pH 8.3), 50 mM KCl, 3.0 mM $MgCl_2$, 0.8 mM each primer, 197 mM deoxynucleoside triphosphates (dNTPs), and 10 U/50 μl *Taq* DNA polymerase (AmpliTaq Gold; Applied Biosystems).

The tissue slides were warmed to 70°C, and 50 μl of the PCR mixture was overlaid onto the proteinase K-treated tissue specimens. An Ampli cover disc with Ampli cover clips (Applied Biosystems) was attached to each specimen. The slides were placed in the GeneAmp *in situ* PCR system 1000 unit at 70°C. PCR was performed at 95°C for 10 min, followed by 35 to 55 cycles at 95°C for 30 s and 60°C for 2 min and a final extension at 72°C for 10 min. Immediately after the PCR, the slides were fixed in 4% paraformaldehyde in phosphate-buffered saline (PBS) for 10 min at 37°C, washed in 2× SSC (1× SSC is 0.15 M NaCl plus 0.015 M sodium citrate) for 2 min, rinsed with distilled water for 2 min, dehydrated in 99.5% ethanol for 1 min, and then air dried. ISH was performed by mixing the DIG-labeled probe (final concentration, 100 ng/ml) with 65 μl of hybridization buffer (50% deionized formamide, 4× SSC, 1× Denhardt's solution [0.2% bovine serum albumin {BSA}, 0.2% polyvinyl pyrrolidone, 0.2% Ficoll 400], 100 μg/ml denatured salmon sperm DNA, 100 μg/ml yeast RNA, and 1 mM EDTA) and then adding the mixture to each section, heating to 97°C for 10 min, and cooling to 37°C in decrements of 1°C/min (27). Hybridization was carried out overnight at 37°C. Stringency washes were conducted with the following: 2× SSC twice for 10 min at 37°C, 0.03× SSC for 10 min at 50°C, 0.1% Triton X-100 in TBS (0.1 M Tris [pH 7.5], 0.1 M NaCl) for 10 min at room temperature, and TBS for 5 min at room temperature. After incubation in blocking reagent (0.1 M Tris

[pH 7.5], 0.1 M NaCl, 10% sheep serum, 3% BSA) at room temperature for 15 min, the slides were covered with 100 μl anti-DIG antibody conjugated with alkaline phosphatase (Roche) and diluted at 1:900 with 1% BSA in TBS at 37°C for 60 min. After this reaction, the slides were washed twice (3 min each) with 0.1% Triton X-100 in TBS, then with TBS alone, and finally with APS (0.1 M Tris [pH 9.0], 0.1 M NaCl, 50 mM $MgCl_2$) at room temperature. The slides were incubated in 100 μl dye solution (338 μg/ml nitroblue tetrazolium chloride [NBT], 175 μg/ml 5-bromo-4-chloro-3-indolyl-phosphate 4-toluidine salt [BCIP], and 450 μM Levamisole [Vector Labs, Burlingame, CA] in APS) at 37°C in the dark. After sufficient color development, they were washed with deionized water for 1 min and then mounted with aqueous mounting medium.

RT-PCR–ISH for detecting HBV RNA. The OCT-embedded frozen sections were placed on glass slides. After proteinase K treatment, the tissue sections were digested with RNase-free DNase I (Roche; diluted to 3 U/μl in 0.1 M sodium acetate and 5 mM $MgSO_4$). The DNase I reaction mixture (66 μl) was overlaid onto the tissue sections, which were then enclosed in a frame. The slides were reacted in an aluminum box at 37°C for 20 min and inactivated at 97°C for 10 min. They were then washed in DEPC-treated water, dehydrated in 99.5% ethanol, and air dried.

Moloney murine leukemia virus (MMLV) reverse transcriptase (10 U/μl; Invitrogen, Carlsbad, CA) was used in a reaction mixture containing 10 mM Tris-HCl (pH 8.3), 50 mM KCl, 5.0 mM $MgCl_2$, 1 μM antisense primer, 1 mM dNTPs, 2 U/μl RNase inhibitor (Takara, Otsu, Japan), and 10 mM dithiothreitol (DTT). The specimens were then overlaid with the mixture, reacted at 42°C for 60 min, washed with distilled water, dehydrated in 99.5% ethanol, and air dried. The subsequent procedures were the same as described for PCR-ISH.

Immunohistochemical staining for detecting HBV proteins. Deparaffinized formaldehyde-fixed sections or fixed frozen liver tissue sections on glass slides were soaked in distilled water, digested with 0.1% pronase (protease P8038 XXIV; Sigma-Aldrich, Tokyo, Japan) for 1 min, and washed with PBS at room temperature. After 30 min of incubation in blocking reagent (1% BSA and 2.5 mM EDTA in PBS) at room temperature, the slides were reacted with 100 μl of anti-HBs and anti-HBc polyclonal antibody solutions for 3 h at room temperature and then overnight at 4°C. The following polyclonal antibodies were used: anti-HBs rabbit polyclonal antibody anti-HBc rabbit polyclonal antibody (Novocastra Laboratories, Newcastle, United Kingdom), or normal rabbit serum diluted in blocking reagent. After the reaction, the slides were washed four times with PBS at room temperature and incubated for 60 min at room temperature in 100 μl anti-rabbit IgG conjugated with peroxidase (Amersham ECL; GE Healthcare, Piscataway, NJ) diluted to 1:100 in blocking reagent. The slides were then washed four times with PBS at room temperature and stained by using 3,3′-diaminobenzidine tetrahydrochloride (DAB) (Vector Labs). Following counterstaining with Mayer's hematoxylin solution, the tissue specimens were dehydrated in 99.5% ethanol and 80% xylene. The slides were sealed by using Bioleit (Oken Shoji, Tokyo, Japan).

RT-PCR–ISH for detecting HCV RNA. HCV RNA was detected by using methods similar to those used for detecting HBV RNA except for the following steps: the DNase I step was omitted, and 1.5 mM $MgCl_2$ was used in the PCR mixture.

Primers and probe sets in RTD-PCR for quantifying HBV DNA, HCV RNA, β-actin DNA, and GAPDH mRNA. The primer sets to quantify the S and X regions of HBV were the same as those used for PCR-ISH. The TaqMan probes for these regions, the primers and probe designed to quantify the 5′-UTR of HCV (33), and those used to quantify β-actin genomic DNA and GAPDH (glyceraldehyde-3-phosphate dehydrogenase) mRNA (internal control) are shown in Table 2. Each PCR comprised 50 cycles (95°C for 30 s, 60°C for 40 s, and 72°C for 30 s) in a real-time PCR system (ABI Prism 7700 sequence detector system; Applied Biosystems).

Amplicor monitor assays. The Amplicor monitor assays were performed as described previously (22, 24, 33, 36).

HE staining. HBV- or HCV-infected deparaffinized formaldehyde-fixed sections or fixed frozen liver tissue sections were stained with hematoxylin and eosin (HE).

LCM of liver tissue. A frozen liver tissue sample was sectioned by using a cryostat and fixed in acetone, followed by HE staining. Laser capture microdissection (LCM) was performed by using an LM 200 system (Olympus, Tokyo, Japan) as described previously (6, 11). This procedure produced approximately 30 hepatocytes from each of three areas (perivenular, intermediate, and periportal) in the section. Total RNA was extracted from the LCM samples, and HCV RNA and GAPDH mRNA were quantified by RTD-PCR.

TABLE 2. Primers and probes for PCR-ISH and RT-PCR

Technique	Virus or protein (region)	Primer or probe		
		Type	Description, nucleotides	Sequence
PCR-ISH	HBV (HBs)	Primer	Forward (HB-166-S21), 166–186	5′-CACATCAGGATTCCTAGGACC-3′
			Reverse (HB-344-R20), 344–325	5′-AGGTTGGTGAGTGATTGGAG-3′
		Probe	(HB-242-S45D), 242–286	5′-(DIG)-CAGAGTCTAGACTCGTGGTGGACTTCTCTCAATTTTCTAGGGGGA-(DIG)n-3′
	HBV (HBx)	Primer	Forward (HB-1584-S21), 1584–1604	5′-CTTCGCTTCACCTCTGCACGT-3′
			Reverse (HB-1744-R23), 1744–1722	5′-CCCAACTCCTCCCAGTCCTTAAA-3′
		Probe	(HB-1705-R45D), 1705–1661	5′-(DIG)-TATGCCTCAAGGTCGGTCGTTGACATTGCTGAGAGTCCAAGAGTC-(DIG)n-3′
RT-PCR–ISH	HCV (5′-UTR)	Primer	Forward (R6-129-S19), 129–147	5′-CCGGGAGAGCCATAGTGGT-3′
			Reverse (R6-290-R19), 290–272	5′-AGTACCACAAGGCCTTTCG-3′
		Probe	(R6-225-S45D), 225–269	5′-(DIG)-ATTTGGGCGTGCCCCCGCGAGACTGCTAGCCGAGTAGTGTTGGGT-(DIG)n-3′
TaqMan	HBV (S)	Probe	Forward (HB-242-S26FT), 242–267	5′-CAGAGTCTAGACTCGTGGTGGACTTC-3′
	HBV (X)	Probe	Forward (HB-1681-S25FT), 1681–1705	5′-TGTCAACGACCGACCTTGAGGCATA-3′
	HCV (5′-UTR)	Primer	Forward (R6-130-S17), 130–146	5′-CGGGAGCCATAGTGG-3′
			Reverse (R6-290-R19), 290–272	5′-AGTACCACAAGGCCTTTCG-3′
		Probe	Forward (R6-148-S21FT), 148–168	5′-CTGCGGAACCGGTGAGTACAC-3′
	β-Actin (genomic DNA)	Primer	Forward (β-ACT-1998-S20), 1998–2017	5′-CAGTGTGACATGGTGCATCT-3′
			Reverse (β-ACT-2246-R24), 2246–2223	5′-GTGAGGATCTTCATGAGGTAGTCA-3′
		Probe	Forward (β-ACT-2063-S22FT), 2063–2084	5′-ACGTTGCTATCCAGGCTGTGCT-3′
	GAPDH	Primer	Forward (GAPDH-514-S24), 514–537	5′-TGCACCACCAACTGCTTAGCACCC-3′
			Reverse (GAPDH-837-R24), 837–814	5′-CTTGATGTCATCATATTTGGCAGG-3′
		Probe	Forward (GAPDH-584-S25FT), 584–608	5′-TGACCACAGTCCATGCCATCACTGC-3′

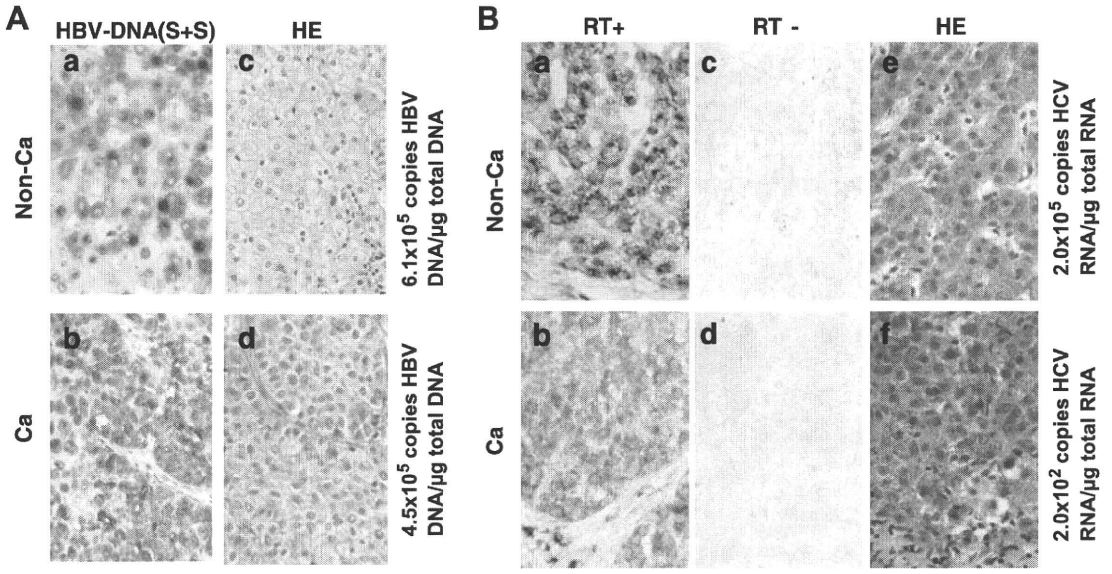

FIG. 1. (A) Panels a and b, HBV DNA detected by PCR-ISH and immunohistochemical staining in noncancerous (Non-Ca) (panel a) and cancerous (Ca) (panel b) liver tissues obtained from a patient infected with HBV. The numbers of PCR cycles were 37 and 42, respectively. Panels c and d, serial sections were stained with HE. Magnification, ×400. S+S, primers and probe targeting the S region of HBV DNA. (B) Panels a and b, HCV RNA detected by RT-PCR–ISH (45 cycles of PCR) in noncancerous (panel a) and cancerous (panel b) tissues obtained from a patient infected with HCV. Panels c and d, no HCV RNA was detected in the RT-negative controls. Panels e and f, serial sections were stained with HE. Magnification, ×400.

RESULTS

Sensitivity and specificity of PCR-ISH versus RTD-PCR for detecting HBV DNA and HCV RNA. PCR-ISH showed positive results for HBV DNA in 10 tissue specimens from eight HBsAg-seropositive patients and two patients whose serum HBV DNA was barely detected by RTD-PCR despite being their HBsAg negative (patients 21 and 22) (Table 1). PCR-ISH yielded negative results for four patients who were negative for serum HBsAg and HCV antibody (patients 23, 24, 28, and 29) and three patients who were negative for serum HBsAg but positive for HCV antibody (patients 9 to 11).

Thirteen of the 14 tissue specimens from the patients with serum HCV antibody had a positive result for HCV RNA by RT-PCR–ISH (sensitivity, 92.9%). In contrast, HCV RNA was not detected by RT-PCR–ISH in four tissue specimens from the patients negative for both HCV antibody and HBsAg (patients 23, 25, 26, and 27) or in the sample from an HBsAg-positive and HCV antibody-negative patient (patient 6).

We performed PCR-ISH and RT-PCR–ISH on the same HBV- or HCV-infected samples from noncancerous and cancerous regions in which we had previously quantitated viral genomic DNA or RNA by RTD-PCR (34). The noncancerous tissue contained 6.1×10^5 copies of HBV DNA/μg total DNA, and the cancerous regions included 4.5×10^5 copies/μg total DNA. Equivalent numbers of cells in the noncancerous and cancerous tissues stained positive for HBV on PCR-ISH (patient 4; Fig. 1A). The PCR-ISH results were consistent with the HBV DNA copy number previously determined by RTD-PCR (34).

Noncancerous tissue from an HCV-positive patient contained 2.0×10^5 copies HCV RNA/μg total RNA, whereas cancerous tissue contained 2.0×10^2 copies/μg total RNA (patient 12; Fig. 1B). HCV RNA was observed by RT-PCR–ISH in hepatocytes of the liver tissue sections from an HCV-infected patient (Fig. 1B). In the noncancerous tissue, an intense hybridization signal was found at the perinuclear sites of almost all the hepatocytes in the section (Fig. 1B, panel a). In contrast, in the cancerous tissue, there was only a weak HCV RNA hybridization signal in the hepatocytes (Fig. 1B, panel b). When the RT step was omitted (control), no HCV RNA was detected in the noncancerous or cancerous tissue sections (Fig. 1B, panels c and d). These results were consistent with the previous quantitation of HCV RNA copy number by RTD-PCR (34).

Detection of HBV DNA by PCR-ISH. HBV DNA was detected by PCR-ISH in the tissue sections obtained from an HBV DNA-seropositive patient. Amplified PCR products were detected by using a probe for either the S or the X region (Fig. 2A, panels a to d) but were not detected by using a heterologous probe (Fig. 2A, panels e and f). Amplification of either the S or the X region of HBV DNA gave the same pattern of hybridization (Fig. 2A, panels a to d). HBV DNA was detected by PCR-ISH in almost all hepatocytes (Fig. 2A, panels a to d) and was very obvious even under low magnification (Fig. 2A, panels a and c). An intense hybridization signal was observed predominantly at the perinuclear site under high magnification (Fig. 2A, panels b and d). In contrast, HBV DNA was not detected by using HBs- and HBx-matched primer and probe combinations in sections obtained from an HBV DNA-seronegative patient (data not shown). DNA fragments amplified by using the S and X region primer sets were 179 bp and 161 bp, respectively (Fig. 2B). Sections from an HBV DNA-seronegative patient were negative in the PCR analysis (data not shown).

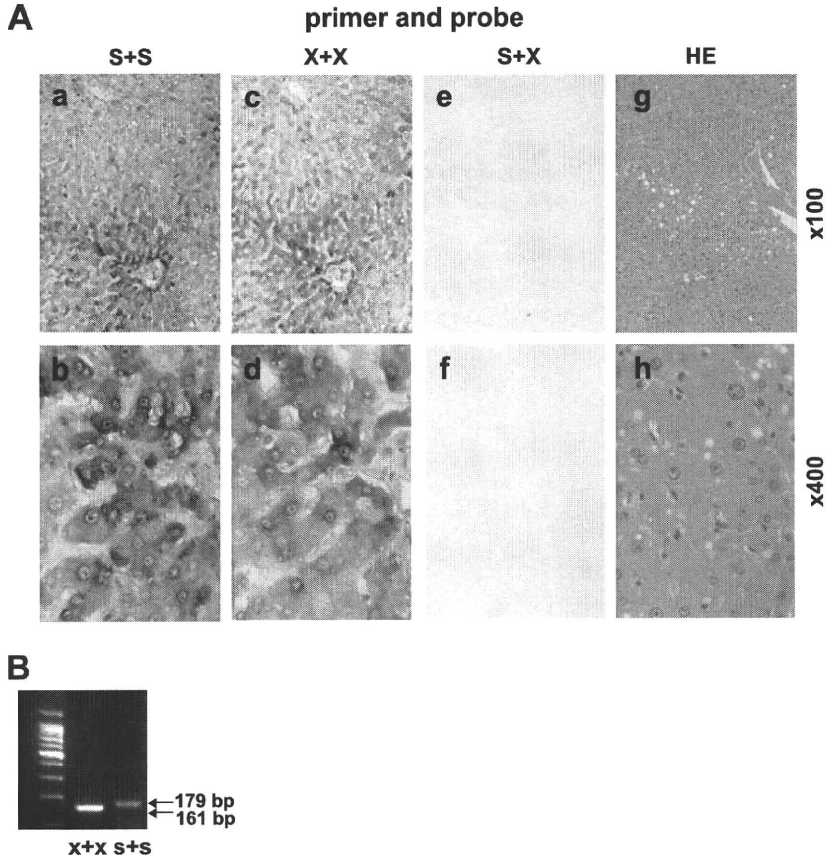

FIG. 2. (A) Panels a to f, HBV DNA detected in liver tissue sections from a patient with chronic hepatitis B by PCR-ISH (42 cycles of PCR). Panels g and h, serial sections were stained with HE. Magnifications, ×100 (panels a, c, e, and g) and ×400 (b, d, f, and h). S+S, primers and probe targeting the S region; X+X, primers and probe targeting the X region; S+X, primers and probe targeting the S and X regions, respectively. (B) Amplified DNA fragments in the PCR mixture of the section in panel A visualized by 3% agarose gel electrophoresis. The PCR product of the X region was 161 bp, and that of the S region was 179 bp.

Localization of HBV DNA, HBV RNA, HBsAg, and HBcAg in liver tissue. HBV DNA, HBV RNA, HBsAg, and HBcAg were detected by PCR-ISH, RT-PCR–ISH, and immunohistochemical staining of serial sections from an HBV-infected patient (patient 5; Fig. 3A, panels a to h). HBV DNA was detected in almost all the hepatocytes by PCR-ISH, although there was wide variation in the hybridization signal intensity between different areas of the section (Fig. 3A, panels a and b). The staining pattern of HBV RNA was similar to that of HBV DNA (Fig. 3A, panels c and d). Intracytoplasmic and intranuclear staining for HBsAg and HBcAg, respectively, was found in some hepatocytes (Fig. 3A, panels f and h). PCR and RT-PCR results were confirmed by gel electrophoresis of the amplified products in the supernatant from the tissue section (Fig. 3B, panels a and b).

Detection of HCV RNA by RT-PCR–ISH. HCV RNA could be detected by RT-PCR–ISH in almost all the hepatocytes in the liver sections obtained from an HCV RNA-seropositive patient (Fig. 4A, panels a and b). Under high magnification, a strong HCV RNA signal was detected in the perinuclear area (Fig. 4A, panel b). A negative-control test (no RT) did not detect any HCV RNA (Fig. 4A, panels c and d). The expected 162-bp DNA fragment amplified by RT-PCR in the supernatant from the tissue section was detected (Fig. 4B, lane 2). In contrast, HCV RNA was not detected in the liver section obtained from an HCV RNA-seronegative patient, regardless of whether RT was used (data not shown).

Isolation of HCV RNA in hepatocytes by LCM. Hepatocyte groups were captured from the perivenular, intermediate, and periportal areas by LCM (Fig. 4C, panel a). HCV RNA was quantified by RTD-PCR in approximately 30 hepatocytes captured by LCM and normalized against the picogram weight of GAPDH mRNA (Fig. 4C, panels b to d); the HCV RNA levels were equivalent in all three regions (Fig. 4C, panel d).

Detection of HCV RNA in the epithelium of the large bile duct. HCV RNA was detected by RT-PCR–ISH in the epithelium of the large bile duct, which was surrounded by dense fibrous and elastic tissue (Fig. 4D, panels a and b). In contrast, no HCV RNA was detected in the epithelium of the small bile duct. Further, HCV RNA was not detected in the portal vein or its branches (Fig. 4D, panel a).

Detection of HBV DNA and HCV RNA in noncancerous and cancerous liver tissue sections obtained from a patient with HBV and HCV coinfection. Figure 5 shows the results for HBV DNA and HCV RNA in liver samples from a patient with HCC having HCV and HBV coinfection. The amounts of serum HBV DNA and HCV RNA were 39 copies/ml and 5×10^7 copies/ml, respectively (patient 21) (34). In the noncancerous

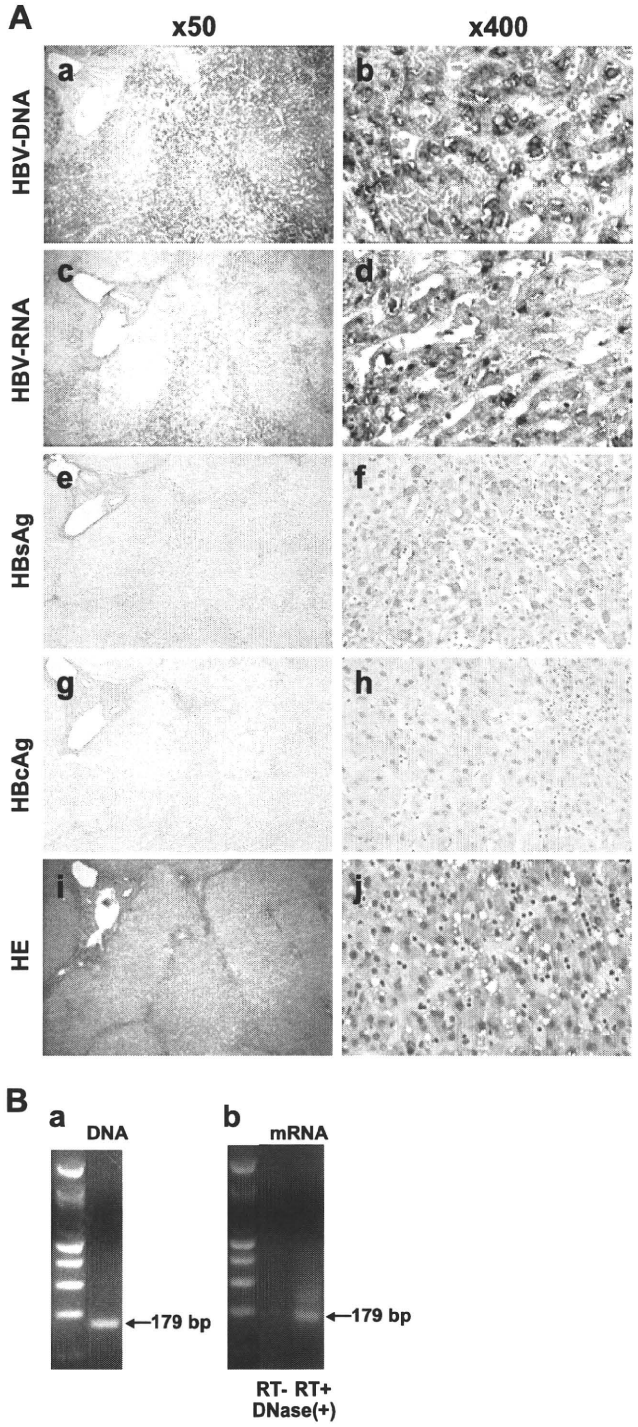

FIG. 3. (A) Panels a to h, HBV DNA, HBV RNA, HBsAg, and HBcAg detected in OCT-embedded frozen liver tissue from a patient with chronic hepatitis B by PCR-ISH (panels a and b), RT-PCR–ISH (panels c and d), and immunohistochemical staining (panels e to h). Panels i and j, HE staining of serial sections. The primers and probe targeted the S region to detect HBV DNA and HBV RNA. Antibodies to the envelope and core proteins were used to detect HBsAg and HbcAg, respectively. Magnifications, ×50 (panels a, c, e, g, and i) and ×400 (panels b, d, f, h, and j). The number of PCR cycles was 42. (B) Amplified DNA fragments in the PCR mixture of the section in panel A. Panel a, the DNA fragments amplified by 42 cycles of PCR were visualized by 3% agarose gel electrophoresis. Panel b, RT-PCR after DNase I treatment (3 U/μl) and negative controls (no RT).

tissue from the patient with HBV and HCV coinfection, there was an intense hybridization signal for HCV RNA on RT-PCR–ISH in almost all the hepatocytes (Fig. 5A, panel b). There was also a positive but weak RT-PCR–ISH signal for HCV RNA in the tumor hepatocytes (Fig. 5B, panel b). Few hepatocytes in the cancerous tissue were positive for HBV DNA by PCR-ISH (Fig. 5B, panel a), and no HBV DNA hybridization signal was detected in the noncancerous tissue (Fig. 5A, panel a).

DISCUSSION

The standard assay for detecting replication of HBV and HCV in tissue is ISH, but results are often inconsistent and sometimes difficult to reproduce. The specificity of ISH is high but its sensitivity low, and it is difficult to detect low copy numbers of the HBV or HCV genome in tissue. PCR technology has been adapted to *in situ* amplification of viral genomes or their replicative intermediates in liver tissue sections, but sensitivity and specificity remain major challenges to the application of this approach (13, 18, 23, 25, 26, 30, 31). Here, we describe the use of a novel, highly specific and sensitive PCR-ISH method to determine the distribution and localization of HBV DNA, HBV RNA, and HCV RNA in both normal and cancerous liver tissues.

PCR-ISH is the most sensitive technology currently available for the detection of viral genomes, but a major potential limitation of this approach is the low specificity. We were able to improve the specificity of PCR-ISH by careful optimization of certain steps. PCR was performed using sets of antisense and sense primers that were complementary to the sequences located in the S and X regions of HBV and the 5′-UTR upstream of the core region of HCV. We added PCR templates to the PCR mixture and then added the PCR mixture to the HBV- or HCV-negative tissue sections. The slides were placed in the GeneAmp *in situ* PCR system 1000 unit, and PCR-ISH was performed as described in Materials and Methods. Following these results, we selected the primer and probe set that did not stain the HBV- or HCV-negative tissue sections by PCR-ISH. Second, the type and concentration of protease and the treatment time were adjusted to optimize permeabilization of membranes and release of protein-nucleic acid cross-linking while avoiding overdigestion. Third, to improve the specificity for detecting viral genomes, we limited the number of PCR cycles and fixed the liver tissue sections in 4% paraformaldehyde immediately after PCR amplification. This step is essential to avoid diffusion of PCR products into neighboring cells, a phenomenon known as the diffusion artifact. Limiting the number of PCR cycles was also important for eliminating the background staining, as too many cycles resulted in high background staining and loss of tissue morphology. Fourth, we added a DIG-dUTP tail at the 3′ ends of the probes for PCR-ISH and RT-PCR–ISH. These 45-mer probes were optimized to improve their sensitivity without impairing the specificity.

HBV DNA was detected by PCR-ISH in a large number of hepatocytes in tissue sections from an HBV DNA-seropositive patient (Fig. 1A, panel a). HBV DNA was also observed by PCR-ISH in tumor hepatocytes in a section of cancerous tissue from the same patient (Fig. 1A, panel b). As shown in Fig. 2A,

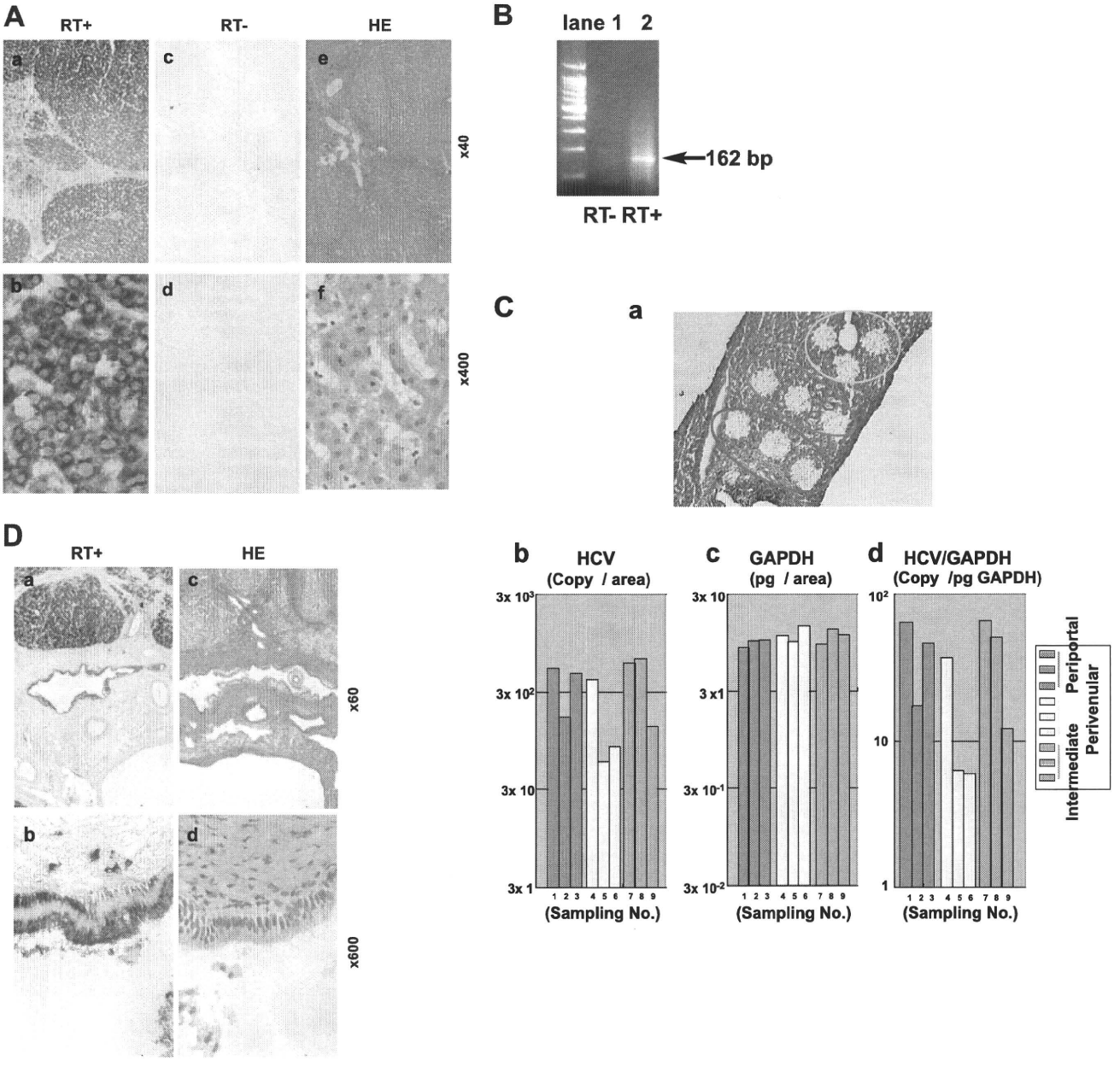

FIG. 4. (A) Panels a and b, HCV RNA detected in liver tissue samples from a patient with chronic hepatitis C by RT-PCR–ISH. Panels c and d, HCV RNA was not detected in a negative control (no RT). The number of PCR cycles was 45. Panels e and f, serial sections were stained with HE. Magnifications, ×40 (panels a, c, and e) and ×400 (panels b, d, and f). (B) DNA fragments in the PCR mixture of the section in panel A were amplified with the RT step and detected by 3% agarose gel electrophoresis. Amplification without the RT step resulted in no detection of DNA fragments. (C) Panel a, after LCM of nine areas, sections of liver tissue obtained from a patient with chronic hepatitis C were stained with HE. Panels b and c, HCV RNA and GAPDH mRNA in each of the areas were quantified by RTD-PCR, and the results are expressed as copy number per LCM area. Panel d, the copy number of HCV RNA was corrected by using the picogram weight of GAPDH. (D) Panels a and b, HCV RNA detected in the epithelium of the large bile duct by RT-PCR–ISH. The number of PCR cycles was 45. Panels c and d, serial sections were stained with HE. Magnifications, ×60 (a and c) and ×600 (b and d).

we obtained clear and reproducible patterns of distribution or localization of the viral genomes in the tissue sections. The visual patterns of HBV DNA distribution were similar, irrespective of the primer sets and probes (Fig. 2A, panels a to d). These data indicate that our technique is highly specific and reproducible for the detection of HBV DNA.

The staining pattern of HBV RNA was similar to that of HBV DNA (Fig. 3A, panels c and d). HBV DNA was also observed by PCR–ISH in tumor hepatocytes in a section of cancerous tissue from an HBV DNA-seropositive patient (Fig. 1A, panel b), but neither HBsAg nor HBcAg was detected in this section (data not shown). As shown in Fig. 3, the intensity of HBV DNA by PCR-ISH was almost the same as that of HBV RNA by RT-PCR–ISH but did not coincide with the

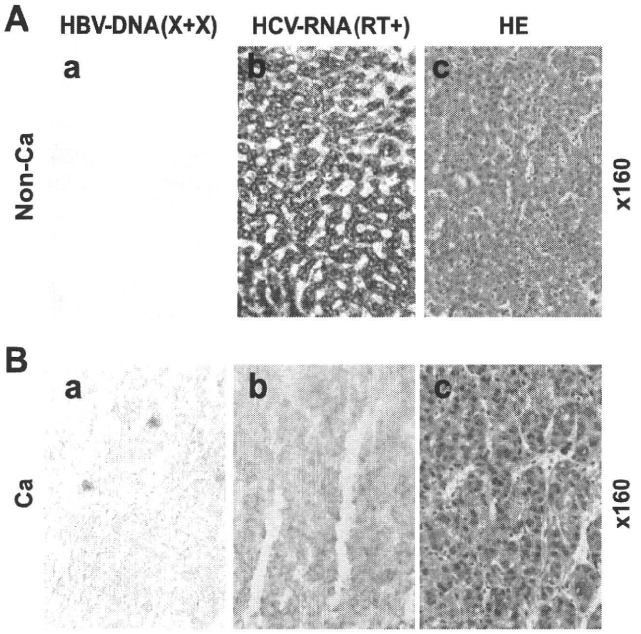

FIG. 5. Panels a and b, HBV DNA (panels a) and HCV RNA (panels b) in noncancerous (non-Ca) (A) and cancerous (Ca) (B) liver tissue obtained from a patient coinfected with HBV and HCV were detected by PCR-ISH (55 cycles of PCR) and RT-PCR–ISH (45 cycles of PCR), respectively. Panels c, serial sections were stained with HE. Magnification, ×160.

intensity of HBV protein expression. HBV has four overlapping open reading frames regulated by two enhancer elements and four promoters (14).

We had reported previously that HCV RNA and HCV core protein levels are relatively stable irrespective of fibrosis (33, 35). In the present study, HCV RNA was detected in almost all hepatocytes in all sections. Furthermore, we emphasize the similar staining pattern of almost all hepatocytes at the cellular level. HCV RNA was detected in the cytoplasm but not in the nucleus. The detection of an intense signal at the perinuclear site may reflect the replication process of HCV (10). HCV RNA was also detected in the epithelium of the large bile duct but not in the endothelial cells, portal tracts, or sinusoidal lymphocytes, which is consistent with the results of previous studies (5, 8). Thus, the epithelium of the large bile duct, but not that of the small duct, can support HCV replication.

We confirmed the specificity for detecting the HCV RNA copy number by quantification in a small area of an LCM section (Fig. 4C); similar amounts of HCV RNA were detected in each area. The detection of HCV RNA in each area by LCM and RTD-PCR excluded the possibility of diffusion of the PCR product by RT-PCR–ISH.

Recent molecular biological techniques have demonstrated low-level HBV viremia in some patients with chronic hepatitis C who were negative for all serological HBV markers. In these cases, HBV DNA not only is integrated in the human chromosomes but also replicates in hepatocytes (34). In the previous study, we measured the levels of HBV DNA and HCV RNA using RTD-PCR with singly infected or coinfected noncancerous and cancerous liver tissues (34). In the case of coinfection, HCV replication was dominant in the noncancerous tissue whereas HBV replication was dominant in the cancerous tissue. Some studies have shown that HCV inhibits HBV gene expression and replication (7, 15).

Using this novel, highly specific and sensitive PCR-ISH method, we could visualize the tissue staining patterns of HBV and HCV, which were consistent with those seen by RTD-PCR. This revealed the novel finding that almost all hepatocytes are infected with HBV or HCV in patients with chronic liver disease, suggesting that the viruses spread throughout the liver in the chronic stage. However, further study with a large number of samples from each stage of infection is needed to clarify the mechanism of persistent infection via our assay method.

ACKNOWLEDGMENTS

We are grateful to Yuichi Hirata of the Tokyo Metropolitan Institute of Medical Science and Kyoko Kohara of Kumamoto University for their critical comments and helpful discussions.

This study was supported by grants from the Ministry of Education, Culture, Sports, Science and Technology of Japan, the Program for Promotion of Fundamental Studies in Health Sciences of the Pharmaceuticals and Medical Devices Agency of Japan, and the Ministry of Health, Labor and Welfare of Japan.

REFERENCES

1. **Abe, A., K. Inoue, T. Tanaka, J. Kato, N. Kajiyama, R. Kawaguchi, S. Tanaka, M. Yoshiba, and M. Kohara.** 1999. Quantitation of hepatitis B virus genomic DNA by real-time detection PCR. J. Clin. Microbiol. **37:**2899–2903.
2. **Beasley, R. P., L. Y. Hwang, C. C. Lin, and C. S. Chien.** 1981. Hepatocellular carcinoma and hepatitis B virus. A prospective study of 22 707 men in Taiwan. Lancet **ii:**1129–1133.
3. **Bedossa, P., and T. Poynard.** 1996. An algorithm for the grading of activity in chronic hepatitis C. The METAVIR Cooperative Study Group. Hepatology **24:**289–293.
4. **Benvegnù, L., G. Fattovich, F. Noventa, F. Tremolada, L. Chemello, A. Cecchetto, and A. Alberti.** 1994. Concurrent hepatitis B and C virus infection and risk of hepatocellular carcinoma in cirrhosis. A prospective study. Cancer **74:**2442–2448.
5. **Boletis, J. N., J. K. Delladetsima, F. Makris, H. Theodoropoulou, S. Vgenopoulou, A. Kostakis, and A. Hatzakis.** 2000. Cholestatic syndromes in renal transplant recipients with HCV infection. Transpl. Int. **13**(Suppl. 1):S375–S379.
6. **Bonner, R. F., M. Emmert-Buck, K. Cole, T. Pohida, R. Chuaqui, S. Goldstein, and L. A. Liotta.** 1997. Laser capture microdissection: molecular analysis of tissue. Science **278:**1481–1483.
7. **Chen, S. Y., C. F. Kao, C. M. Chen, C. M. Shih, M. J. Hsu, C. H. Chao, S. H. Wang, L. R. You, and Y. H. Lee.** 2003. Mechanisms for inhibition of hepatitis B virus gene expression and replication by hepatitis C virus core protein. J. Biol. Chem. **278:**591–607.
8. **Delladetsima, J. K., F. Makris, M. Psichogiou, A. Kostakis, A. Hatzakis, and J. N. Boletis.** 2001. Cholestatic syndrome with bile duct damage and loss in renal transplant recipients with HCV infection. Liver **21:**81–88.
9. **Di Bisceglie, A. M., S. E. Order, J. L. Klein, J. G. Waggoner, M. H. Sjogren, G. Kuo, M. Houghton, Q. L. Choo, and J. H. Hoofnagle.** 1991. The role of chronic viral hepatitis in hepatocellular carcinoma in the United States. Am. J. Gastroenterol. **86:**335–338.
10. **El-Hage, N., and G. Luo.** 2003. Replication of hepatitis C virus RNA occurs in a membrane-bound replication complex containing nonstructural viral proteins and RNA. J. Gen. Virol. **84:**2761–2769.
11. **Emmert-Buck, M. R., R. F. Bonner, P. D. Smith, R. F. Chuaqui, Z. Zhuang, S. R. Goldstein, R. A. Weiss, and L. A. Liotta.** 1996. Laser capture microdissection. Science **274:**998–1001.
12. **Fattovich, G.** 2003. Natural history and prognosis of hepatitis B. Semin. Liver Dis. **23:**47–58.
13. **Fragulidis, G. P., R. E. Cirocco, D. Weppler, M. Berho, G. Gillian, M. Markou, A. Viciana, V. Esquenazi, J. R. Nery, J. Miller, K. R. Reddy, and A. G. Tzakis.** 1998. In situ enzymatic oligonucleotide amplification of hepatitis C virus-RNA in liver biopsy specimens (reverse transcriptase in situ polymerase chain reaction) after orthotopic liver transplantation for hepatitis C-related liver disease. Transplantation **66:**1472–1476.
14. **Ganem, D., and A. M. Prince.** 2004. Hepatitis B virus infection—natural history and clinical consequences. N. Engl. J. Med. **350:**1118–1129.
15. **Guo, H., T. Zhou, D. Jiang, A. Cuconati, G.-H. Xiao, T. M. Block, and J.-T. Guo.** 2007. Regulation of hepatitis B virus replication by the phosphatidylinositol 3-kinase-akt signal transduction pathway. J. Virol. **81:**10072–10080.

16. **Holland, P. V., and H. J. Alter.** 1975. The clinical significance of hepatitis B virus antigens and antibodies. Med. Clin. North Am. **59:**849–855.
17. **Kiyosawa, K., T. Sodeyama, E. Tanaka, Y. Gibo, K. Yoshizawa, Y. Nakano, S. Furuta, Y. Akahane, K. Nishioka, R. H. Purcell, et al.** 1990. Interrelationship of blood transfusion, non-A, non-B hepatitis and hepatocellular carcinoma: analysis by detection of antibody to hepatitis C virus. Hepatology **12:**671–675.
18. **Komminoth, P., A. A. Long, R. Ray, and H. J. Wolfe.** 1992. In situ polymerase chain reaction detection of viral DNA, single-copy genes, and gene rearrangements in cell suspensions and cytospins. Diagn. Mol. Pathol. **1:**85–97.
19. **Kuo, G., Q. L. Choo, H. J. Alter, G. L. Gitnick, A. G. Redeker, R. H. Purcell, T. Miyamura, J. L. Dienstag, M. J. Alter, C. E. Stevens, et al.** 1989. An assay for circulating antibodies to a major etiologic virus of human non-A, non-B hepatitis. Science **244:**362–364.
20. **Large, M. K., D. J. Kittlesen, and Y. S. Hahn.** 1999. Suppression of host immune response by the core protein of hepatitis C virus: possible implications for hepatitis C virus persistence. J. Immunol. **162:**931–938.
21. **Leone, N., and M. Rizzetto.** 2005. Natural history of hepatitis C virus infection: from chronic hepatitis to cirrhosis, to hepatocellular carcinoma. Minerva Gastroenterol. Dietol. **51:**31–46.
22. **Navas, S., and V. Carreno.** 1995. Semiquantification by Amplicor assay of hepatitis C virus genome during therapy. J. Hepatol. **22:**115–117.
23. **Negro, F.** 1998. Detection of hepatitis C virus RNA in liver tissue: an overview. Ital. J. Gastroenterol. Hepatol. **30:**205–210.
24. **Nolte, F. S., C. Thurmond, and M. W. Fried.** 1995. Preclinical evaluation of AMPLICOR hepatitis C virus test for detection of hepatitis C virus RNA. J. Clin. Microbiol. **33:**1775–1778.
25. **Nuovo, G. J., F. Gallery, P. MacConnell, J. Becker, and W. Bloch.** 1991. An improved technique for the in situ detection of DNA after polymerase chain reaction amplification. Am. J. Pathol. **139:**1239–1244.
26. **Nuovo, G. J., P. MacConnell, A. Forde, and P. Delvenne.** 1991. Detection of human papillomavirus DNA in formalin-fixed tissues by in situ hybridization after amplification by polymerase chain reaction. Am. J. Pathol. **139:**847–854.
27. **Sansonno, D., V. Cornacchiulo, V. Racanelli, and F. Dammacco.** 1997. In situ simultaneous detection of hepatitis C virus RNA and hepatitis C virus-related antigens in hepatocellular carcinoma. Cancer **80:**22–33.
28. **Schluger, L. K., P. A. Sheiner, S. N. Thung, J. Y. Lau, A. Min, D. C. Wolf, I. Fiel, D. Zhang, M. A. Gerber, C. M. Miller, and H. C. Bodenheimer, Jr.** 1996. Severe recurrent cholestatic hepatitis C following orthotopic liver transplantation. Hepatology **23:**971–976.
29. **Seeger, C., and W. S. Mason.** 2000. Hepatitis B virus biology. Microbiol. Mol. Biol. Rev. **64:**51–68.
30. **Shieh, B., S.-E. Lee, Y.-C. Tsai, I.-J. Su, and C. Li.** 1999. Detection of hepatitis B virus genome in hepatocellular carcinoma tissues with PCR-in situ hybridization. J. Virol. Methods **80:**157–167.
31. **Shin, Y. J., S. W. Cho, K. B. Hahm, Y. S. Kim, J. H. Kim, K. H. Park, and S. I. Lee.** 1998. Localization of hepatitis B virus DNA in hepatocellular carcinoma by polymerase chain reaction in situ hybridization. J. Korean Med. Sci. **13:**377–382.
32. **Shiratori, Y., S. Shiina, P. Y. Zhang, E. Ohno, T. Okudaira, D. A. Payawal, S. K. Ono-Nita, M. Imamura, N. Kato, and M. Omata.** 1997. Does dual infection by hepatitis B and C viruses play an important role in the pathogenesis of hepatocellular carcinoma in Japan? Cancer **80:**2060–2067.
33. **Takeuchi, T., A. Katsume, T. Tanaka, A. Abe, K. Inoue, K. Tsukiyama-Kohara, R. Kawaguchi, S. Tanaka, and M. Kohara.** 1999. Real-time detection system for quantification of hepatitis C virus genome. Gastroenterology **116:**636–642.
34. **Tanaka, T., K. Inoue, Y. Hayashi, A. Abe, K. Tsukiyama-Kohara, H. Nuriya, Y. Aoki, R. Kawaguchi, K. Kubota, M. Yoshiba, M. Koike, S. Tanaka, and M. Kohara.** 2004. Virological significance of low-level hepatitis B virus infection in patients with hepatitis C virus associated liver disease. J. Med. Virol. **72:**223–229.
35. **Tanaka, T., J. Y. Lau, M. Mizokami, E. Orito, E. Tanaka, K. Kiyosawa, K. Yasui, Y. Ohta, A. Hasegawa, S. Tanaka, et al.** 1995. Simple fluorescent enzyme immunoassay for detection and quantification of hepatitis C viremia. J. Hepatol. **23:**742–745.
36. **Zeuzem, S., B. Rüster, and W. K. Roth.** 1994. Clinical evaluation of a new polymerase chain reaction assay (Amplicor HCV) for detection of hepatitis C virus. Z Gastroenterol. **32:**342–347.

JOURNAL OF VIROLOGY, Nov. 2010, p. 11761–11770 Vol. 84, No. 22
0022-538X/10/$12.00 doi:10.1128/JVI.00638-10

Sphingomyelin Activates Hepatitis C Virus RNA Polymerase in a Genotype-Specific Manner▽†

Leiyun Weng,[1] Yuichi Hirata,[2] Masaaki Arai,[3] Michinori Kohara,[2] Takaji Wakita,[4] Koichi Watashi,[4,5] Kunitada Shimotohno,[5,6] Ying He,[7] Jin Zhong,[7] and Tetsuya Toyoda[1]*

Units of Viral Genome Regulation[1] and Viral Hepatitis,[7] Institut Pasteur of Shanghai, Key Laboratory of Molecular Virology and Immunology, Chinese Academy of Sciences, 411 Hefei Road, 200025 Shanghai, People's Republic of China; Department of Microbiology and Cell Biology, Tokyo Metropolitan Institute of Medical Biology, 3-18-22 Honkomagome, Bunkyo-Ku, Tokyo 113-8613, Japan[2]; Pharmacology Laboratory, Pharmacology Department V, Mitsubishi Tanabe Pharma Corporation, 1000 Kamoshida-cho, Aoba-ku, Yokohama 227-0033, Japan[3]; Department of Virology II, National Institute of Health, 1-23-1 Toyama, Shinjuku, Tokyo 132-8640, Japan[4]; Laboratory of Human Tumor Viruses, Department of Viral Oncology, Institute for Virus Research, Kyoto University, Kyoto 606-8507, Japan[5]; and Chiba Institute of Technology, 2-17-1 Tsudamuna, Narashino, Chiba 275-0016, Japan[6]

Received 25 March 2010/Accepted 27 August 2010

Hepatitis C virus (HCV) replication and infection depend on the lipid components of the cell, and replication is inhibited by inhibitors of sphingomyelin biosynthesis. We found that sphingomyelin bound to and activated genotype 1b RNA-dependent RNA polymerase (RdRp) by enhancing its template binding activity. Sphingomyelin also bound to 1a and JFH1 (genotype 2a) RdRps but did not activate them. Sphingomyelin did not bind to or activate J6CF (2a) RdRp. The sphingomyelin binding domain (SBD) of HCV RdRp was mapped to the helix-turn-helix structure (residues 231 to 260), which was essential for sphingomyelin binding and activation. Helix structures (residues 231 to 241 and 247 to 260) are important for RdRp activation, and 238S and 248E are important for maintaining the helix structures for template binding and RdRp activation by sphingomyelin. 241Q in helix 1 and the negatively charged 244D at the apex of the turn are important for sphingomyelin binding. Both amino acids are on the surface of the RdRp molecule. The polarity of the phosphocholine of sphingomyelin is important for HCV RdRp activation. However, phosphocholine did not activate RdRp. Twenty sphingomyelin molecules activated one RdRp molecule. The biochemical effect of sphingomyelin on HCV RdRp activity was virologically confirmed by the HCV replicon system. We also found that the SBD was the lipid raft membrane localization domain of HCV NS5B because JFH1 (2a) replicon cells harboring NS5B with the mutation A242C/S244D moved to the lipid raft while the wild type did not localize there. This agreed with the myriocin sensitivity of the mutant replicon. This sphingomyelin interaction is a target for HCV infection because most HCV RdRps have 241Q.

Hepatitis C virus (HCV) has a positive-stranded RNA genome and belongs to the family *Flaviviridae* (21). HCV chronically infects more than 130 million people worldwide (34), and HCV infection often induces liver cirrhosis and hepatocellular carcinoma (19, 28). To date, pegylated interferon (PEG-IFN) and ribavirin are the standard treatments for HCV infection. However, many patients cannot tolerate their serious side effects. Therefore, the development of new and safer therapeutic methods with better efficacy is urgently needed.

Lipids play important roles in HCV infection and replication. For example, the HCV core associates with lipid droplets and recruits nonstructural proteins and replication complexes to lipid droplet-associated membranes which are involved in the production of infectious virus particles (24). HCV RNA replication depends on viral protein association with raft membranes (2, 30). The association of cholesterol and sphingolipid with HCV particles is also important for virion maturation and infectivity (3). The inhibitors of the sphingolipid biosynthetic pathway, ISP-1 and HPA-12, which specifically inhibit serine palmitoyltransferase (SPT) (23) and ceramide trafficking from the endoplasmic reticulum (ER) to the Golgi apparatus (37), suppress HCV virus production in cell culture but not viral RNA replication by the JFH1 replicon (3). Other serine SPT inhibitors (myriocin and NA255) inhibit genotype 1b replication (4, 29, 33). Very-low-density lipoprotein (VLDL) also interacts with the HCV virion (15).

Sakamoto et al. reported that sphingomyelin bound to HCV RNA-dependent polymerase (RdRp) at the sphingomyelin binding domain (SBD; amino acids 230 to 263 of RdRp) to recruit HCV RdRp on the lipid rafts, where the HCV complex assembles, and that NA255 suppressed HCV replication by releasing HCV RdRp from the lipid rafts (29). In the present study, we analyzed the effect of sphingomyelin on HCV RdRp activity *in vitro* and found that sphingomyelin activated HCV RdRp activity in a genotype-specific manner. We also determined the sphingomyelin activation domain and the activation mechanism. Finally, we confirmed our biochemical data by a HCV replicon system.

* Corresponding author. Mailing address: Unit of Viral Genome Regulation, Institut Pasteur of Shanghai, Chinese Academy of Sciences, 411 Hefei Road, 200025 Shanghai, People's Republic of China. Phone and fax: 86 21 6385 1621. E-mail: ttoyoda@amber.plala.or.jp.

† Supplemental material for this article may be found at http://jvi.asm.org.

▽ Published ahead of print on 15 September 2010.

MATERIALS AND METHODS

HCV RNA polymerase. A C-terminal 21-amino-acid deletion was made to the HCV RdRps of strains HCR6 (genotype 1b) (36), NN (1b) (35), Con1 (1b) (5), JFH1 (2a) (36), J6CF (2a) (25), H77 (1a) (7), and RMT (1a), and the mutants

were purified from bacteria as described previously (36). HCR6 (1b) RdRp with the mutation L245A [RdRp(L245A)] or I253A [RdRp(I253A)] or the double mutation L245A and I253A [RdRp(L245A/I253A)]; JFH1 (2a) RdRp with the mutation(s) A242C/S244D, A242, S244D, or T251Q; J6CF (2a) RdRp with the mutation(s) R241Q, S244D, or R241Q/S244D; and H77 (1a) RdRp(A238S/Q248E) were introduced using an *in vitro* mutagenesis kit (Stratagene) and the oligonucleotides listed in Table S1 in the supplemental material. HCR6 (1b) His_6-tagged RdRp(L245A/I253A) was removed from pET21b/KM (36) and cloned into the BamHI/XhoI site of pGEX-6P-3 (GE), resulting in pGEXHCVHCR6RdRp(L245A/I253A).

***In vitro* HCV transcription.** *In vitro* HCV transcription was performed as described previously (36). Briefly, following 30 min of preincubation without ATP, CTP, or UTP, 100 nM HCV RdRp was incubated in 50 mM Tris-HCl (pH 8.0), 200 mM monopotassium glutamate, 3.5 mM $MnCl_2$, 1 mM dithiothreitol (DTT), 0.5 mM GTP, 50 μM ATP, 50 μM CTP, 5 μM [α-^{32}P]UTP, 200 nM RNA template (SL12-1S), 100 U/ml human placental RNase inhibitor, and the lipid (amount indicated below) at 29°C for 90 min. ^{32}P-labeled RNA products were subjected to 6% polyacrylamide gel electrophoresis (PAGE) containing 8 M urea. The resulting autoradiograph was analyzed with a Typhoon Trio plus image analyzer (GE).

RNA filter binding assay. An RNA filter binding assay was performed as described previously (36). Briefly, 100 nM HCV RdRp and 100 nM ^{32}P-labeled RNA template (SL12-1S) were incubated with or without 0.01 mg/ml egg yolk sphingomyelin in 25 μl of 50 mM Tris-HCl (pH 7.5), 200 mM monopotassium glutamate, 3.5 mM $MnCl_2$, and 1 mM DTT at 29°C for 30 min. After incubation, the solutions were diluted with 0.5 ml of TE (50 mM Tris-HCl [pH 7.5], 1 mM EDTA) buffer and filtered through nitrocellulose membranes (0.45-μm pore size; Millipore). The filter was washed five times with TE buffer, and the bound radioisotope was analyzed by Typhoon Trio plus after being dried.

Enzyme-linked immunosorbent assay (ELISA). Ninety-six-well microtiter plates (Corning) were coated with 250 ng of egg yolk sphingomyelin in ethanol by evaporation at room temperature. After the wells were blocked with phosphate-buffered saline (PBS) and 3% bovine serum albumin (BSA), they were incubated with 1 pmol of the HCV RdRp of HCR6 (1b) wild type (wt) or L245A, I253A, or L245A/I253A mutant; NN (1b); H77 (1a); RMT (1a); J6CF (2a); or JFH1 (2a) wt or A242C/S244D, A242, S244D, or T251Q mutant in Tris-buffered saline (50 mM Tris-HCl [pH 7.5] and 150 mM NaCl) for 1.5 h at room temperature. After being blocked with 3% BSA, the bound HCV RdRp was detected by adding rabbit anti-HCV RdRp serum (1:5,000) (see Fig. S1 in the supplemental material) (17) before incubation with a horseradish peroxidase (HRP)-conjugated anti-rabbit IgG antibody (1:5,000; Southern Biotech). The optical density at 450 nm (OD_{450}) was measured with a Spectra Max 190 spectrophotometer (Molecular Devices) using a TMB (3,3′,5,5′-tetramethylbenzidine) Liquid Substrate System (Sigma).

HCV subgenomic replicon. A D244S mutation was introduced into the HCV strain NN (1b) subgenomic replicon pLMH14 (35), resulting in pLMH(NN)5B(D244S) [where 5B(D244S) is the NS5B protein with the mutation D244S]. The A242C/S244D mutation was introduced into the HCV JFH1 (2a) replicon, pSGR-JFH1/luc (25), resulting in pSGR-JFH1/luc5B(A242C/S244D). The HpaI and XbaI fragment of pSGR-JFH1 (18) was replaced with that of pSGR-JFH1/luc5B(A242C/S244D), resulting in pSGR-JFH15B(A242C/S244D). The A238S/Q248E mutation was introduced into HCV H77 (1a) replicon pHCVrep13(S2204I)/Neo (7) after the neomycin gene was replaced by the firefly luciferase gene [pH77(I)/luc] by insertion of AflII and AscI sites (see Table S1 in the supplemental material), resulting in pH77(I)/luc5B(A238S/Q248E). Subgenomic replicon RNA was transcribed *in vitro* by T7 RNA polymerase using MegaScript (Ambion) after the replicon plasmids were linearized by XbaI (strain NN and JFH1 replicons) or HpaI (strain H77 replicon). Subgenomic replicon RNA was stored at −80°C after being purified by phenol-chloroform extraction and ethanol precipitation.

Replicon assay with myriocin. Huh7.5.1 cells were kindly provided by F. Chisari and were maintained in Dulbecco's modified Eagle's medium (DMEM; Gibco) with 10% fetal bovine serum (FBS; Gibco) (38). HCV replicon RNA (10 μg) was transfected into 4 × 10^6 Huh7.5.1 cells (1 × 10^7/ml) in OptiMEM I (Gibco) by electroporation (GenePulser Xcell; Bio-Rad) at 270 V, 100 Ω, and 950 μF. After transfection, the cells were plated in 12-well plates incubated in DMEM–10% FBS. At 6 h after transfection, cells were treated with 0, 5, and 50 nM myriocin. At 4, 54, and 78 h after transfection (48 and 72 h after myriocin treatment), the cells were harvested, and luciferase activity was measured using a Dual-Glo luciferase assay kit and a GloMax 96 Microplate Luminometer (Promega). Luciferase activity was normalized against the activity at 4 h after transfection (26).

HCV JFH1 wt and NS5B(A242C/S244D) replicon cells. Huh7/scr cells were kindly provided by F. Chisari of the Scripps Research Institute and were maintained in Dulbecco's modified Eagle's medium (Gibco) with 10% fetal bovine serum (Gibco). RNA (10 μg each) from SGR-JFH1 and SGR-JFH1 with the mutations A242C/S244D in NS5B [NS5B(A242C/S244D) was transfected into 4 × 10^6 Huh7/scr cells (1 × 10^7/ml) in OptiMEM I (GIBCO) by electroporation (GenePulser Xcell; Bio-Rad) at 270 V, 100 Ω, and 950 μF. After transfection, the cells were plated in 10-cm dishes and incubated in DMEM–10% FBS with 1.0 and 0.5 mg/ml G418 (Gibco). JFH1 wt and NS5B(A242C/S244D) replicon cells were maintained in DMEM–10% FBS and 0.5 mg/ml G418.

Membrane floating assay. JFH1 wt and NS5B(A242C/S244D) replicon cells were suspended in two packed cell volumes of hypotonic buffer (10 mM HEPES-NaOH [pH 7.6], 10 mM KCl, 1.5 mM $MgCl_2$, 2 mM DTT, and 1 tablet/25 ml of EDTA-free protease inhibitor cocktail tablets [Roche]) and disrupted by 30 strokes of homogenization in a Dounce homogenizer using a tight-fitting pestle at 4°C. After nuclei were removed by centrifugation at 2,000 rpm for 10 min at 4°C, the supernatant (postnuclear supernatant [PNS]) was treated with 1% Triton X-100 in TNE buffer (25 mM Tris-HCl [pH 7.6] 150 mM NaCl, 1 mM EDTA) for 30 min on ice. The lysates were supplemented with 40% sucrose and centrifuged at 38,000 rpm in a Beckman SW41 Ti rotor (Beckman Coulter) overlaid with 30% and 10% sucrose in TNE buffer at 4°C for 14 h.

Western blotting. Western blotting using anti-HCV RdRp (17), rabbit anti-NS3 (32), anti-NS5A (16) and anti-caveolin-2 was performed as previously published (17).

Reagent. Egg yolk sphingomyelin, cholesterol phosphocholine, myriocin, and rabbit anti-caveolin-2 antibodies were purchased from Sigma. Hexanoyl sphingomyelin, C_6-ceramide, C_8-β-D-glucosyl ceramide, and C_8-β-D-lactosyl ceramide were purchased from Avanti Polar Lipids. [α-^{32}P]UTP was purchased from New England Nuclear.

Statistical analysis. Significant differences were evaluated using *P* values calculated from a Student's *t* test.

Nucleotide sequence accession number. The sequence of HCV RMT has been deposited in the GenBank under accession number AB520610.

RESULTS

Sphingomyelin activation of HCV RNA polymerases of various genotypes. There are several sequence variations in the sphingomyelin binding domain (SBD; amino acids 231 to 260 of HCV RdRp) among HCV genotypes (see Fig. 7A). In order to compare the RdRps of different genotypes of HCV, we purified RdRp from genotypes 1b (strains HCR6, NN, and Con1), 1a (H77 and MRT), and 2a (JFH1 and J6CF) (see Fig. S2 in the supplemental material). First, the effect of ethanol on HCV HCR6 (1b) RdRp transcription was examined because lipids were suspended in ethanol before they were added to the HCV transcription reaction mixture. We found that 2% ethanol did not inhibit HCV transcription (see Fig. S3 in the supplemental material); therefore, all subsequent experiments were performed using less than 2% ethanol.

The kinetics of sphingomyelin activation were analyzed using egg yolk sphingomyelin for HCR6 (1b) RdRp wt (Fig. 1A) and subtype 2a (JFH1 and J6CF) RdRps (Fig. 1B), and *N*-hexanoyl-D-*erythro*-sphingosylphosphorylcholine (hexanoyl sphingomyelin) was used for HCR6 (1b) RdRp wt (Fig. 1C) and subtype 1a (H77 and RMT) RdRps (Fig. 1D). The egg yolk sphingomyelin activation curve of HCR6 (1b) RdRp wt at low concentrations (<0.01 mg/ml) was sigmoid. The transcription activity of HCR6 (1b) RdRp wt increased in a dose-dependent manner. It was activated 11-fold at 0.01 mg/ml and then plateaued (14-fold activation) at 0.1 mg/ml. However, JFH1 (2a) and J6CF (2a) RdRps were activated 2.5-fold and 2.2-fold, respectively, at 0.01 mg/ml sphingomyelin, at which point they plateaued.

Egg yolk sphingomyelin is a mixture. In order to obtain the optimal molar ratio for sphingomyelin activation of HCR6 (1b)

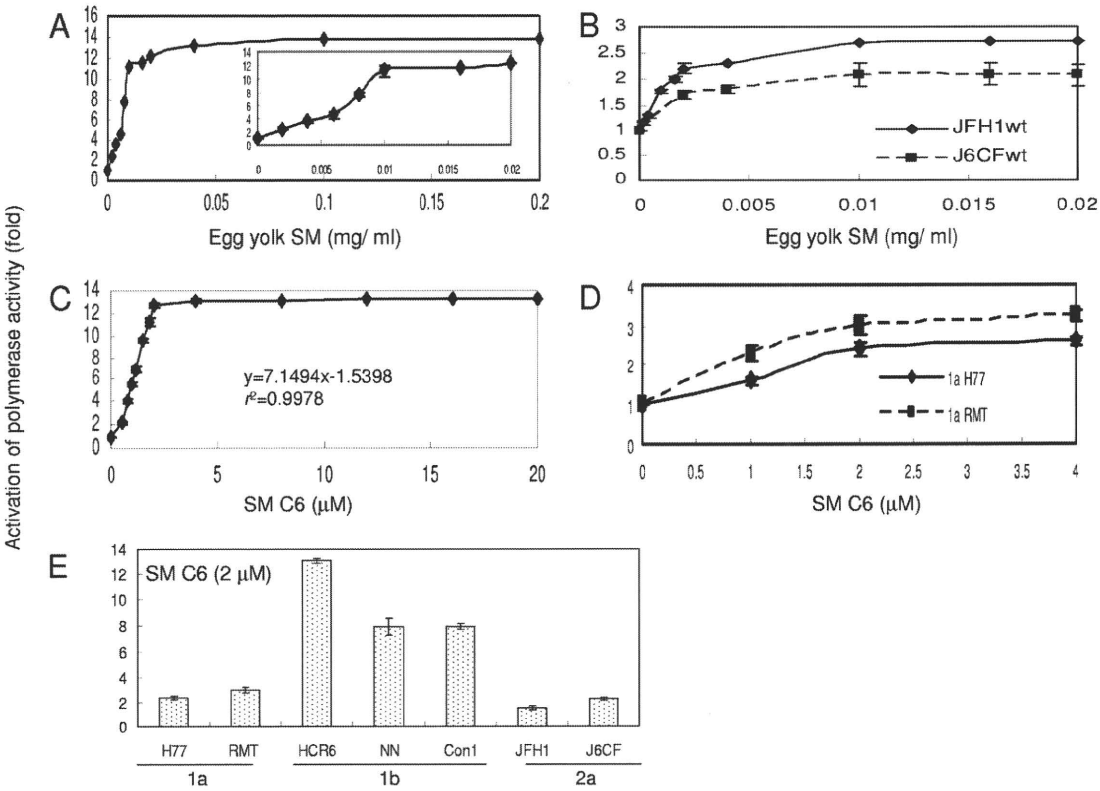

FIG. 1. Sphingomyelin activation of HCV RNA polymerases. (A) Activation kinetics of HCV HCR6 (1b) RdRp wt by egg yolk sphingomyelin (SM). The inset shows activation produced by 0 to 0.02 mg/ml egg yolk sphingomyelin. Activation kinetics of HCV 2a (JFH1 and J6CF) RdRps by egg yolk sphingomyelin (B) and of HCV HCR6 (1b) RdRp wt by hexanoyl sphingomyelin (SM C6) (C). In panel C, the first order of the graph was fitted by linear regression; the calculated equation is indicated in the graph. (D) Activation kinetics of HCV 1a (H77 and RMT) RdRps by hexanoyl sphingomyelin. (E) Activation effect of hexanoyl sphingomyelin on HCV RdRp of various genotypes. HCV RdRp (100 nM) was incubated with or without 2 μM SM C6. The names of the RdRps are indicated below the graph. Mean ± standard deviation of the activation ratio was calculated from three independent experiments.

RdRp wt, its activation kinetics were calculated using hexanoyl sphingomyelin (Fig. 1C, SM C6). The equation for the first-order ratio of hexanoyl sphingomyelin activation according to linear regression fitting was as follows: $y = 7.1494x - 1.5398$, where y is the activation ratio and x is the sphingomyelin concentration ($r^2 = 0.9978$). RdRp activation had almost plateaued at 2 μM hexanoyl sphingomyelin. The activation kinetics of JFH1 (2a) and J6CF (2a) RdRps in egg yolk sphingomyelin were biphasic and plateaued at 0.01 mg/ml. Those of RMT (1a) and H77 (1a) RdRps in hexanoyl sphingomyelin were also biphasic and plateaued at 2 μM. The curve of the first order was fitted by linear regression. The molar ratio of RdRp to hexanoyl sphingomyelin at its plateau was calculated as 1:20.

Because RdRp activation had almost plateaued at 2 μM hexanoyl sphingomyelin, we compared the effect of sphingomyelin on 100 M concentrations of RNA polymerases of the HCV 1a, 1b, and 2a genotypes using 2 μM hexanoyl sphingomyelin (Fig. 1E and Table 1).

Helix-turn-helix structure for sphingomyelin binding and activation. Sphingomyelin binds to the SBD peptide (see HCV SBD in Fig. 7) (29). Initially, we tested whether SBD was the sphingomyelin binding site in HCV RdRp by ELISA (Fig. 2A and Table 1). When the L245 and I253 residues of the SBD peptide were mutated to A, sphingomyelin binding activity was lost (29). We introduced the same mutations in HCV HCR6 (1b) RdRp and purified HCR6 (1b) RdRp with mutations L245A, I253A, and L245A/I253A. Because the C-terminal His-tagged HCR6 RdRp(L245A/I253A) was not soluble, it was solubilized by tagging of glutathione *S*-transferase (GST) sequence at the N terminus but lost polymerase activity. As the L245A/I253A mutant had lost its polymerase activity, polymerase activation was tested only for L245A and I253A (Fig. 2B and Table 1). These results confirmed that SBD located in the finger domain (residues 230E to 263G) successfully achieved sphingomyelin binding in HCV RdRp and that sphingomyelin did not bind to the SBD when the helix-turn-helix structure had been destroyed by the L245A or I253A mutation (29).

The sphingomyelin binding activities of genotype 1a and 2a RdRps were also tested (Fig. 2 and Table 1). Both JFH1 and J6CF were tested for genotype 2a because J6CF (2a) RdRp had an additional amino acid difference at position 241 in the SBD, and its sphingomyelin binding activity was very low (Fig. 2A and 7A; Table 1). J6CF (2a) RdRp(R241Q) showed the same sphingomyelin binding activity as HCR6 (1b) RdRp wt, indicating that 241Q was the critical amino acid for sphingomyelin binding. J6CF (2a) RdRp(S244D) and RdRp(R241Q/S244D) also showed higher sphingomyelin binding activity

TABLE 1. Summary of sphingomyelin activation of HCV RNA polymerase activities

Parameter	Value for the parameter by RdRp genotype, strain, and variant[a]																								
	1b									1a							2a								
	HCR6					NN	Con1	RMT	H77			J6CF				JFH1									
	wt	L245A	I253A	L245A/I253A	D244S	wt	wt	wt	wt	A238S/Q248E	wt	R241Q	S244D	R241Q/S244D	wt	A242C	S244D	A242C/S244D	T251Q
SM binding (%)[b]	100	24.3	30.8	15.5	78.7	93.4	117	144	86.7	82.5	19.3	118	53.1	80.2	70.4	75.5	93.1	92.4	80.7
Activation of polymerase (*n*-fold)[c]	13.0 (11.2)[d]	(2.8)[d]	(2.5)[d]	ND	3.6	7.9	7.9	3.0	2.0	8.1	2.3	4.3	5.6	3.4	1.6	1.0	3.1	4.4	1.8
Activation of RNA binding (*n*-fold)[c]	4.5	2.6	1.7	ND	1.9	ND	ND	ND	1.4	3.3	1.5	3.6	3.2	1.7	1.3	ND	ND	1.4	ND

[a] Numbers were averaged from three independent experiments. ND, not done.
[b] Egg yolk sphingomyelin (SM; 250 ng) was used.
[c] Hexanoyl sphingomyelin (2 μM) was used.
[d] Egg yolk sphingomyelin (0.01 mg/ml) was used.

than the wt ($P < 0.001$) but lower binding than the R241Q mutant. However, S244D showed higher RdRp activation than R241Q ($P < 0.005$), while the RdRp activation ratio of the double mutant (R241Q/S244D) was lower than that of S244D or R241Q, although all of them activated RdRp with sphingomyelin ($P < 0.005$) (Fig. 2A and C and Table 1). For JFH1, when the JFH1 RdRp SBD was modified (A242C/S244D) to allow it to bind with more sphingomyelin than the wt ($P < 0.005$), the mutant JFH1 RdRp(A242C/S244D) was activated more than the wt by sphingomyelin ($P < 0.005$) (Fig. 2A and C; Table 1). The sphingomyelin binding activity of JFH1 RdRp(T251Q) was 80.7% of that of HCR6 (1b), and its activation ratio was 1.8-fold. These results agree that SBD is both the sphingomyelin activation and binding domain and that the domains for these two activities are somehow different.

We determined which amino acid, 242C or 244D, enhanced sphingomyelin binding by comparing HCR6 (1b) and JFH1 (2a) RdRps. Sphingomyelin binding of HCR6 (1b) RdRp(D244S) was 79% of that of the wt ($P < 0.005$) (Fig. 2A and Table 1), and its activation by sphingomyelin was only 3.6-fold (Fig. 2C and Table 1). The sphingomyelin binding of JFH1 (2a) RdRp(A242C) and RdRp(S244D) increased to 75.5% and 93.1%, respectively, of HCR6 (1b) RdRp wt (Fig. 2A and Table 1). This was significantly higher than that of JFH1 (2a) RdRp wt ($P < 0.005$), and the sphingomyelin activation of JFH1 (2a) RdRp(A242C) and RdRp(S244D) was increased 1.0-fold and 3.1-fold, respectively ($P < 0.005$) (Fig. 2C and Table 1). From these mutation analyses of the J6CF and JFH1 RdRps, we concluded that 244D enhanced sphingomyelin binding and RdRp activation.

HCV 1a RdRps were not activated even though sphingomyelin bound to them (Fig. 1E and 2A and Table 1). We then tried to elucidate the domains responsible for sphingomyelin activation. There are 14 amino acids (residues 19, 25, 81, 111, 120, 131, 184, 270, 272, 329, 436, 464, 487, and 540) unique to genotype 1a RdRp in the region of residues 1 to 570 and two amino acid differences unique to 1a RdRp in SBD, i.e., 238A and 248Q (see Fig. 6A). Initially, we focused on the SBD and introduced the A238S and Q248E mutations into the H77 (2a) RdRp SBD (Fig. 2A and D and Table 1). The sphingomyelin binding activity of H77 (2a) RdRp(A238S/Q248E) was similar to that of H77 (2a) RdRp wt. The sphingomyelin activation ratio of H77 (2a) RdRp(A238S/Q248E) was increased 8.1-fold, leading us to conclude that these mutations are essential to sphingomyelin activation.

Effect of lipids on HCV RNA polymerase activity. In order to elucidate the structure of the lipids involved in activation of HCV RdRp, D-lactosyl-β-1,1′-*N*-octanoyl-D-*erythro*-sphingosine [C_8-lactosyl(β) ceramide], D-glucosyl-β1-17-N-octanoyl-D-*erythro*-sphingosine (C_8-β-D-glucosyl ceramide), *N*-hexanol-D-*erythro*-sphingosine (C_6-ceramide), and cholesterol were tested for their abilities to activate RdRp. The relative polymerase activities of 100 nM HCV HCR6 (1b) RdRp activated with 0.01 mg/ml egg yolk sphingomyelin, 2 μM hexanoyl sphingomyelin, 8 μM C_8-lactosyl(β) ceramide, 12 μM C_8-β-D-glucosyl ceramide, 12 μM C_6-ceramide, and 0.02 mg/ml cholesterol were 11.2, 13.0, 5.66, 4.19, 1.12, and 2.25 of that without lipids, respectively (Fig. 3A). The amount of lipids that gave the maximum activation was calculated from the kinetics of the lipids bound to HCR6 (1b) and JFH1 (2a) RdRps (Fig. 3B and

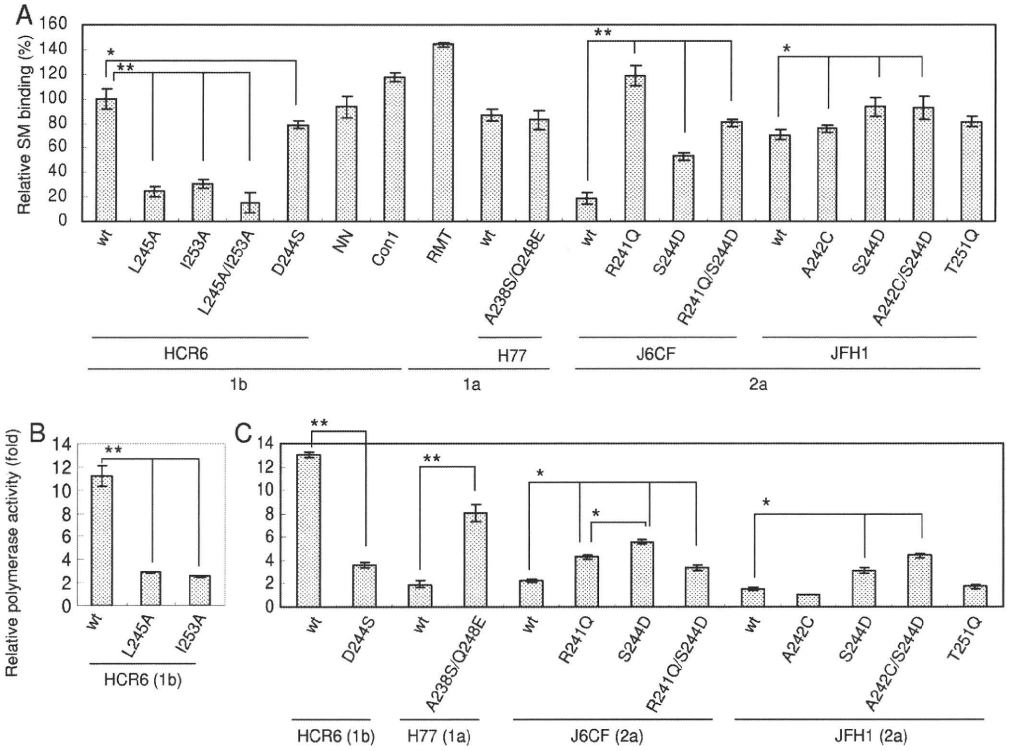

FIG. 2. Sphingomyelin binding and activation of HCV RNA polymerase sphingomyelin binding domain mutants. Names of RdRps are indicated below the graphs. (A) Egg yolk sphingomyelin (SM) binding activity relative to that of HCR6 (1b) RdRp wt. Mean ± standard deviation of the binding was calculated from three independent experiments. (B) Egg yolk sphingomyelin activation of HCR6 (1b) RdRps. RdRps (100 nM) were incubated with or without 0.01 mg/ml egg yolk sphingomyelin. (C) Hexanoyl sphingomyelin activation of the RdRps (RdRp names are indicated below the graphs). HCV RdRps (100 nM) were incubated with or without 2 μM hexanoyl sphingomyelin. The mean ± standard deviation of the activation ratio was calculated from three independent experiments. *, $P < 0.005$; ** $P < 0.001$.

C). C_8-lactosyl(β) ceramide and C_8-β-D-glucosyl ceramide activated HCR6 (1b) RdRp compared with the linear regression kinetics of the reaction with hexanoyl sphingomyelin as it plateaued (Fig. 1C and 3B). Cholesterol activated HCR6 (1b) RdRp slightly but did not activate JFH1 (2a) RdRp (Fig. 3C). We therefore concluded that the phosphocholine of sphingomyelin bound to the SBD of HCV RdRp because the order of HCV RdRp activation was hexanoyl sphingomyelin > C_8-lactosyl(β) ceramide > C_8-β-D-glucosyl ceramide, and C_6-ceramide did not activate HCV HCR6 (1b) RdRp. The polarity of the phosphocholine of sphingomyelin is important for HCV RdRp activation (see Fig. S5 in the supplemental material).

In order to test whether phosphocholine activated HCV RdRp (Fig. 3D), HCR6 (1b) RdRp was incubated with 0.4, 2, 20, 100, and 400 μg and 2, 4, 11, 54, and 100 mg of phosphocholine. Up to 400 μg of phosphocholine did not affect RdRp activity, but more than 2 mg of phosphocholine inhibited RdRp activity.

Effect of sphingomyelin on the template RNA binding of HCV RNA polymerase. The mechanism of HCV RdRp activation was analyzed. RNA polymerase changes its conformation throughout the different transcription steps, and template binding is the first step of transcription (9). Therefore, the effect of sphingomyelin on template RNA binding activity was tested (Fig. 4A and Table 1). Sphingomyelin enhanced the template RNA binding of HCR6 (1b) RdRp wt but not that of JFH1 (2a), H6CF (2a), or H77 (1a) wt RdRp. When the A238S/Q248E mutation was introduced into H77 (1a) RdRp, the RNA binding was enhanced. J6CF (2a) RdRp R241Q and S244D mutants showed similar enhancement of RNA binding, but the R241Q/S244D double mutant did not. The activation effect of RNA binding of HCR6 (1b) RdRp mutants L245A, I253A, and D244S was lower than that of RdRp wt. JFH1 (2a) RdRp wt and RdRp(A242C/S244D) showed similar RNA binding activation levels. Based on a comparison of the sphingomyelin activation of HCR6 (1b) RdRp wt and its mutants which lost sphingomyelin binding with J6CF (2a) RdRp wt and the R241Q and S244D mutants and H77 (1a) RdRp wt and the A238S/Q248E mutant, we concluded that polymerase activation by sphingomyelin was induced mainly via activation of the template RNA binding of RdRp. RNA binding activity of JFH1 (2a) RdRp wt and RdRp(A242C/S244D) was almost saturated because RNA binding of these RdRps was not activated by sphingomyelin (see Fig. S4 in the supplemental material).

HCV RdRp has to be bound with sphingomyelin before or at the same time as it binds to template RNA. After RdRp had bound to the template RNA, sphingomyelin did not enhance template RNA binding strongly (Fig. 4B).

Effect of the sphingomyelin binding domain mutations for HCV replicon activity with myriocin. In order to confirm sphingomyelin activation of HCV polymerase activity in a viral replication system, HCV replicon activity of the loss-of-function mutant HCV NN (1b) NS5B(D244S) and the gain-of-

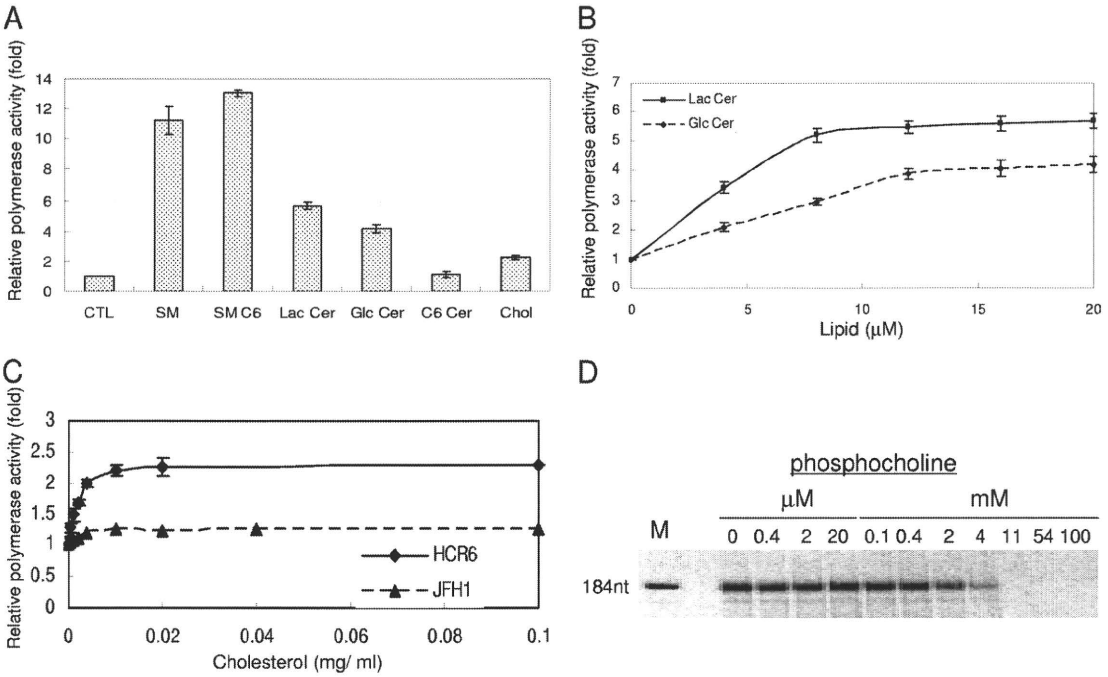

FIG. 3. HCV RNA polymerase activation effect of lipids. (A) Lipid activation of HCR6 (1b) RdRp wt. HCV HCR6 (1b) RdRp wt (100 nM) was incubated with or without (control [CTL]) 0.01 mg/ml egg yolk sphingomyelin (SM), 2 μM hexanoyl sphingomyelin (SM C6), 8 μM C_8-lactosyl(β) ceramide (Lac Cer), 12 μM C_8-β-D-glucosyl ceramide (Glc Cer), 12 μM C_6-ceramide (C6 Cer), or 0.02 mg/ml cholesterol (chol). (B) Activation kinetics of C_8-lactosyl(β) ceramide (Lac Cer) and C_8-β-D-glucosyl ceramide (Glc Cer) on HCR6 (1) RdRp. (C) Activation kinetics of cholesterol on HCR6 (1b) and JFH1 (12a) RdRps. (D) The effect of phosphocholine on HCR6 (1b) RdRp. The mean ± standard deviation of the activation ratio was calculated from three independent experiments.

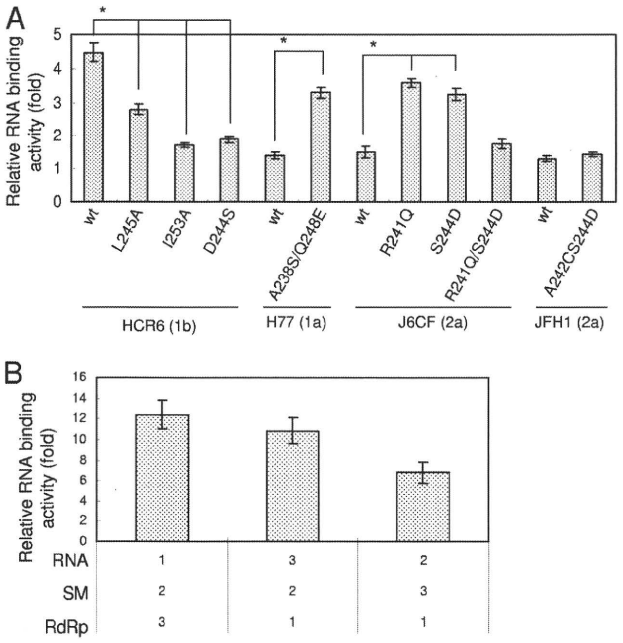

FIG. 4. Sphingomyelin activation of the RNA binding activity of HCV RNA polymerase. (A) Sphingomyelin activation of RNA filter binding of HCV RdRps (RdRp names are indicated below the graph). RdRps and ^{32}P-labeled RNA template (SL12-1S) were incubated with or without egg yolk sphingomyelin (SM), before filtration. (B) Effect of the order of sphingomyelin treatment. Numbers below the graph indicate the order in which the reagents were added. The graph represents the ratio to RNA binding without sphingomyelin. The mean ± standard deviation of the activation ratio was calculated from three independent experiments. *, $P < 0.01$.

function mutants H77 (1a) NS5B(A238S/Q248E) and JFH1 (2a) NS5B(A242C/S244D) were compared with 5 and 50 nM myriocin treatment for 72 h (Fig. 5).

First, HCV replicon activity was compared as the relative luciferase activity (Fig. 5A). Both JFH1 (2a) wt and NS5B(A242C/S244D) replicons showed similar and strong replicon activity ($133 \times 10^3 \pm 12 \times 10^3$ and $138 \times 10^3 \pm 8.5 \times 10^3$, respectively). JFH1 (2a) wt replicon was resistant to myriocin treatment, as reported by Aizaki et al. using other SPT inhibitors (3). The JFH1 (2a) NS5B(A242C/S244D) replicon became sensitive to myriocin but still showed higher replicon activity than NN (1b) or H77 (1a) replicons even at 50 nM myriocin.

To analyze the effect of mutations precisely, the replicon activity relative to each wt strain was compared (Fig. 5B). The JFH1 (2a) wt replicon with 50 nM myriocin showed the same luciferase activity as the wt without myriocin (102% ± 9.6%). JFH1 (2a) NS5B(A242C/S244D) replicon activity was the same as that of the wt without myriocin (103% ± 12%); with 5 nM myriocin it was 84.1% ± 6.6% of the wt level, but with 50 nM myriocin it was 70.3% ± 5.3% of the wt level, which was significantly lower ($P < 0.01$). NN (1b) wt replicon activity was 45.3% ± 6.6% with 5 nM myriocin and 21.7% ± 2.9% with 50 nM myriocin relative to the wt level without myriocin. NN (1b) NS5B(D244S) replicon activity was 72.2% ± 12% without myriocin ($P < 0.05$), 44.0% ± 7.4% with 5 nM myriocin, and 38.1% ± 4.2% with 50 nM myriocin relative to wt level without myriocin, which was significantly higher ($P < 0.01$). Thus, NN (1b) NS5B(D244S) showed lower replicon activity than the wt

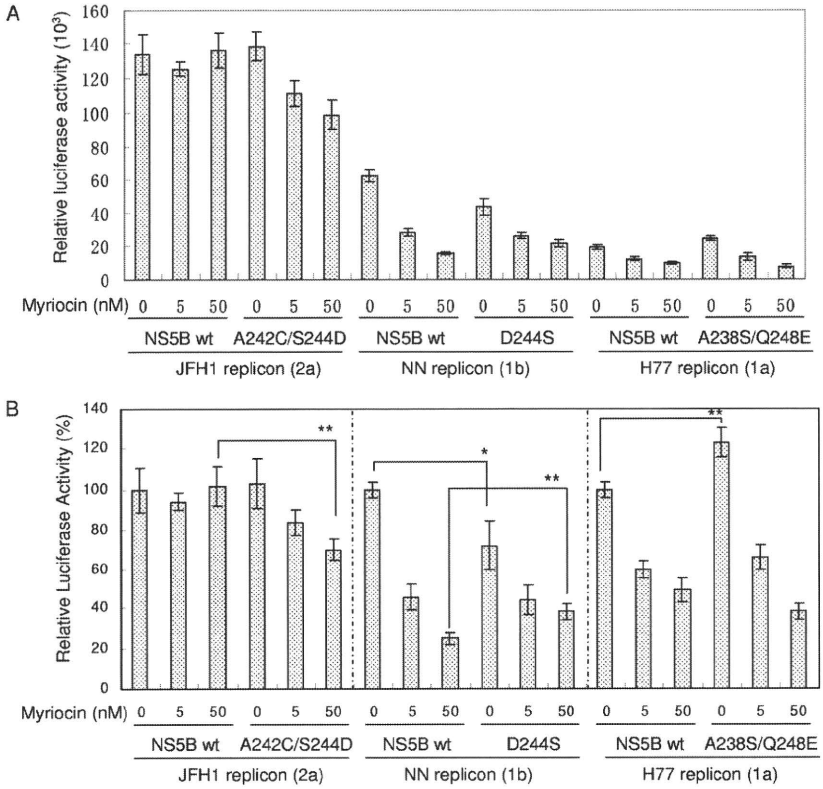

FIG. 5. Myriocin inhibition of HCV replicon activity. Huh7.5.1 cells were incubated with myriocin after transfection with the HCV replicons indicated below the graphs. Means ± standard deviations of the relative luciferase activity at 72 h after myriocin treatment compared to activity at 4 h after transfection (A) and to that of each wt without myriocin (B) were calculated from three independent measurements. *, $P < 0.05$; ** $P < 0.01$.

and was less sensitive to myriocin than the wt. H77 (1a) wt replicon activity was 59.9% ± 4.2% with 5 nM myriocin and 49.2% ± 6.4% with 50 nM myriocin relative to the wt level without myriocin. H77 (1a) NS5B(A238S/Q248E) replicon activity was 123% ± 7.1% without myriocin ($P < 0.01$), 66.1% ± 6.3% with 5 nM myriocin, and 38.0% ± 4.1% with 50 nM myriocin relative to wt level without myriocin. Both H77 (1a) wt and NS5B(A238S/Q248E) replicons were sensitive to myriocin, and the replicon activity of NS5B(A238S/Q248E) was higher than that of the wt.

JFH1 (2a) RdRp(A242C/S244D) localized in the DRM fractions. Myriocin sensitivity of JFH1 (2a) NS5B(A242C/S244D) replicon indicates the importance of 244D in JFH1 NS5B for sphingomyelin binding. To further confirm the role of 244D for recruitment of HCV RdRp to the detergent-resistant membrane (DRM), where the HCV replication complex exists, we compared the distribution of NS5A and NS5B of JFH1 (2a) wt and NS5B(A242C/S244D) in their replicon cells by sucrose density gradient centrifugation of the DRM (Fig. 6). NS5A proteins of both JFH1 (2a) wt and NS5B(A242C/S244D) replicons localized in the DRM fraction where caveolin-2 was present (11, 27), but most of NS5B wt localized in the Triton-soluble fractions. NS5B of JFH1 (2a) NS5B(A242C/S244D) replicon was shifted to the DRM fraction from the soluble fraction. The shift of NS5B(A242C/S244D) localization into the DRM demonstrated that SBD was the DRM localization domain of NS5B and that residue 244D was important for this localization.

DISCUSSION

Hepatitis C virus is an envelope virus, and the lipid components of the virion play important roles in HCV infectivity and virion assembly (3, 15, 20, 24). HCV replication complexes localize in lipid raft structures/DRMs in the membrane frac-

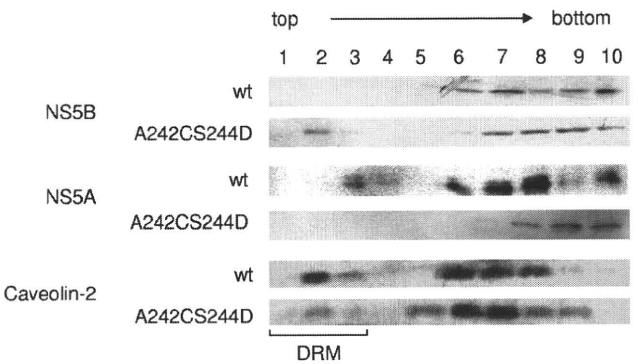

FIG. 6. Membrane floating assay of JFH1 wt and NS5B(A242C/S244D) replicon cells. The PNS fractions of HCV JFH1 (2a) wt and NS5B(A242C/S244D) replicon cells were treated with 1% Triton X-100 in TNE buffer for 30 min at 4°C and subjected to 10 to 40% sucrose gradient centrifugation in TNE buffer. Each fraction was subjected to 10% SDS-PAGE, followed by Western blotting with anti-NS5A, -NS5B, and -caveolin-2 antibodies. Fractions are numbered as indicated at the top of the panel. The DRM fractions (fractions 1 to 3) are indicated.